Dynamic Weighing of Non-Singulated Objects Using a Grid of Decoupled Platforms

by

Bilal Maassarani

A thesis
presented to the University of Waterloo
in fulfillment of the
thesis requirement for the degree of
Master of Applied Science
in
Electrical and Computer Engineering

Waterloo, Ontario, Canada, 2017

I hereby declare that I am the sole author of this thesis. This is a true copy of the thesis, including any required final revisions, as accepted by my examiners.

I understand that my thesis may be made electronically available to the public.

Abstract

Weighing systems exist in various sizes and forms to meet the persistent demand for measuring the mass of objects. Current solutions do not offer a system that can dynamically weigh packages moving in a non-singulated and non-spaced fashion, common in automated settings. In such environments, currently items are singulated which results in a slower flow, increased cost and space requirements. In this work, we propose a design in which small-sized conveyors are mounted on load cells in a grid formation to dynamically weigh non-singulated objects that meet some minimal spacing requirements between them. In the design, moving packages are tracked with a vision system, and an algorithm is formulated to estimate mass based on filtered load cell outputs. Each element of the grid is modelled as a mass-spring-damper system in order to simulate the expected load cell output for the moving objects. A discrete time-variant low-pass filter is adopted from literature to filter the signal and an algorithm is devised to produce a mass estimate. A parameter estimation technique and a simple averaging method which ignore transients are implemented as well for performance comparison. The results are verified experimentally in two proof-of-concept experiments for a full scale prototype. When tuned properly, the time-variant filter succeeds in giving an estimate within a mean of 0.02% error of the rated load cell capacity at speeds up to 0.6 m/s. This is good performance since it does not exceed the rated error for the load cells. The other two estimation methods fail to meet the accuracy requirement at speeds above 0.4 m/s. Potential design considerations and concerns are discussed. Further development and testing is required before the machine can become legal-for-trade.

Acknowledgements

I would like to thank God for giving me the ability to finish this work. I am grateful for the advice and support I received from my supervisors Professors Soo Jeon and Dana Kulić. I would also like to thank Purolator Inc. for collaborating with us on the project by providing the problem that motivated the research, funding and help purchasing parts. I received help from my dear friends Mingu Kwon and Mengxi Zhu who were part of the project. Mingu was hired as an intern and he mainly contributed to the design of the conveyor belts. We purchased the package dimensioning camera system from Mengxi, who founded a company called Tricolops Technologies that offers such systems. Mengxi also provided support in order for us to integrate the camera with the system. I received some assistance in day-to-day tasks from our interns and undergraduate research assistants Atpouthan Paskaran, Chunshang Li and Michael Ru. My friend Tom Wilks, who works in technical sales for HBM Australia, gave me some tips about constructing small belt conveyor scales and choosing load cells. Many thanks to all the people mentioned and anyone with small contributions that I may have missed!

To my loved ones

Table of Contents

List of Tables

List of Figures

Chapter 1

Introduction

1.1 Motivation

Trade can be traced back to prehistoric times as evident from archaeological findings and continues to be of importance as a crucial part of economies [1]. With the exchange of goods comes the need to quantify the products at hand to determine their value and cost of transportation. Early recorded civilisations, such as the ancient Egyptians, Greeks and Romans, all developed metrological systems and weighing technologies. It may be claimed that the oldest balance in the world dates back to 5000 BC. The balance was discovered at the Naqada prehistoric site in Egypt [2]. The most common metrics used in commerce and logistics, along with many other fields, are dimensions and weight. This motivated the standardization and design of various techniques and instruments for the purpose of measurement and weighing. To accommodate today's fast-paced automated environments, the basic manual methods of using measuring tape and mechanical balances have evolved to become faster, more compact, more accurate and have a higher throughput. Examples of such instruments include in-motion laser scanners and checkweighers (see Figures 1.1 and 1.2).

Figure 1.1: 3D Laser Scanner [3] © 2016 Proto3000.

Figure 1.2: In-Motion C3000 Checkweigher [4] © 2014 Mettler-Toledo.

Purolator Inc. is a Canadian integrated freight and parcel solutions provider [5]. A major Purolator facility is its distribution center (or the hub) where a large amount of packages go through a sorting system. The system consists of an integrated conveyor system with multiple diverting pathways connecting the unloading ports to the destination loading ports [6]. To ensure correct sorting and delivery, the sorting system is equipped with various identification instruments which include dimensioners, barcode readers, vision cameras, and/or checkweighers (or in-motion scales).

Unlike other sensory devices, measuring weight requires the singulation of the object. Each package has to be separated from the others so that it can be loaded, individually, on a short section of the conveyor supported by a scale (the middle conveyor belt in Figure

1.2 for example). This causes the weight measurement station to become a bottleneck. For this reason, Purolator has been measuring only the volumetric weight (i.e. the dimensions) of each package and relying on customer-claimed weight as the physical weight. While this is not a problem for ground transportation where the weight may not be a major issue compared to its volume, it becomes a significant issue for air freight where the transportation cost is determined by the gross weight. Therefore, there is a need to develop a checkweigher (or any other instrument) that can dynamically measure the weight of a package moving in a non-singulated and non-spaced environment (see Figure 1.3). This allows a higher throughput improving the overall efficiency of the facility. In this work, the system developed performs this weighing in a non-singulated environment with minimal spacing. In other words, the packages do not have to be placed individually on a single weighing platform to be weighed, but they do have to be somewhat spaced unlike the scenario shown in Figure 1.3.

Figure 1.3: A Non-singulated and Non-spaced Environment at UPS Chicago Area Consolidation Hub [7].

1.2 Background

There are different types of dynamic weighing systems. In this section, we will use the categorization outlined in [8] and [9], which is done based on the principle of operation of such weighing systems. The information presented in this section is based on these works as well. A brief overview of each category, above the line drawn in Figure 1.4, is summarized with emphasis on catch weighing, since it is the closest category to the novel weighing solution we created.

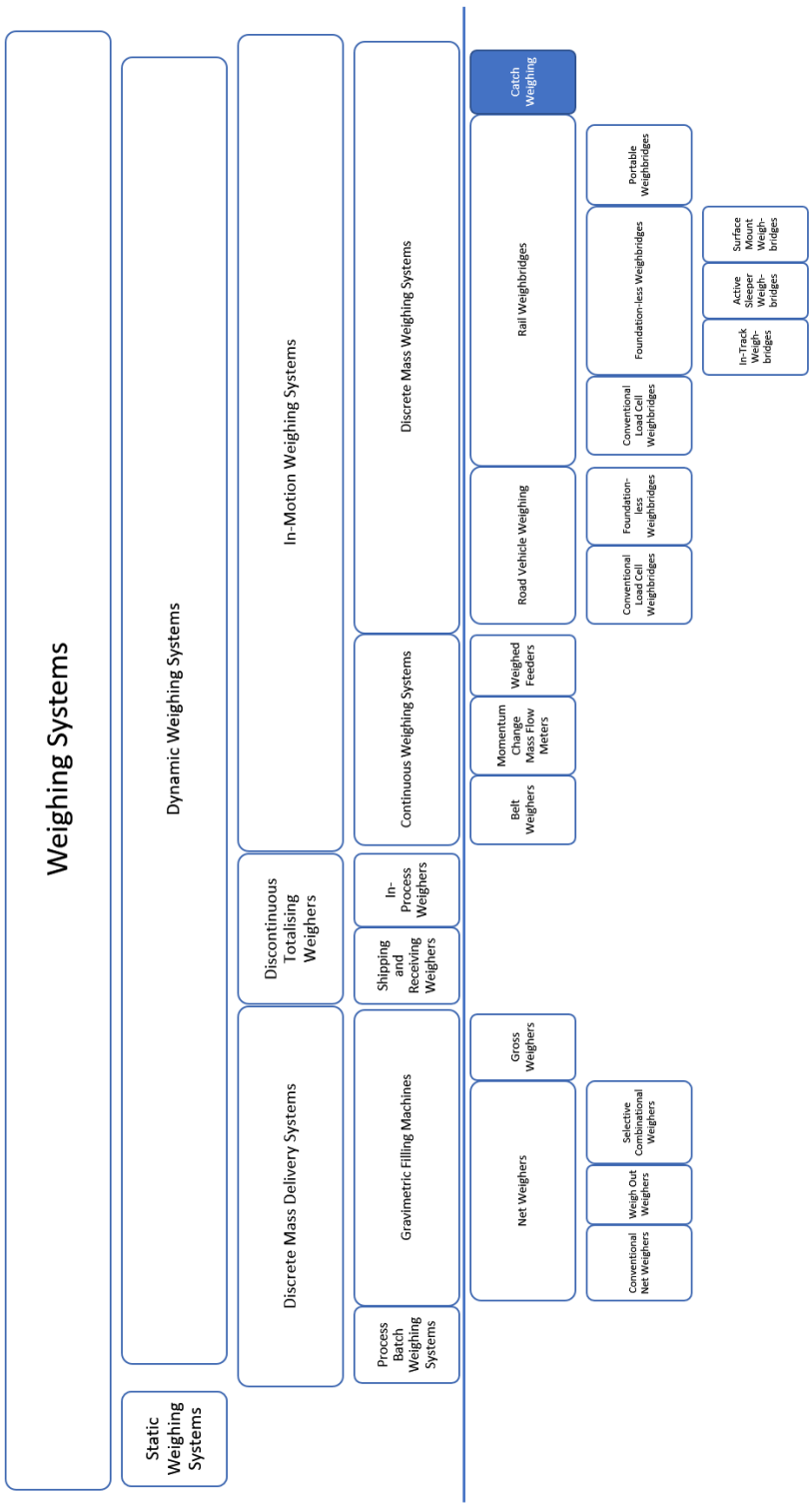

Figure 1.4: Categorization of Weighing Systems.

1. **Discrete mass delivery systems.**

   Discrete, or discontinuous, mass delivery systems are characterized by the mechanism of weighing individual batches of material. These batches may contain pre-packaged goods or pre-mixed materials in the form of powders, granules, lumps or liquids. A variety of dynamic weighing machines that measure such products are classified under this category.

   (a) **Process Batch Weighing Systems.**

   In industries such as pharmaceuticals, food, animal feed, chemical, mineral, fertilizer, rubber & plastics, and glass, it is convenient to divide materials into separate batches. This allows the control of weights and mixing quality. The machine consists of a single or multiple weigh vessels that are supported by load cells for weighing and controlled input/output valves. A controller ensures the vessel is filled with the desired amount of material before unloading. Each vessel may have multiple ingredient inputs and these inputs can be controlled manually, automatically or a combination of both. The batching process that uses multiple feeds per hopper is called cumulative batching. It has the benefit of saving cost and space at the expense of rate of production. On the other hand, the simultaneous batching technique offers a higher accuracy, better mixing and throughput since it weighs material simultaneously rather than sequentially. Of course, this comes at the inconvenience of integrating more equipment. Figure 1.5 shows an example of such a system. The technique involves feeding multiple hoppers which in turn feed other one(s). The third technique is combination batching which combine both techniques and their benefits. It is also beneficial if weighing each ingredient separately is desired before mixing them in the next stage.

Figure 1.5: Simultaneous Process Batching Weighing System [10].
© LIAD Weighing and Control Systems Ltd

(b) **Gravimetric Filling Machines.**

Filling machines fill containers, such as bags, drums and Semi Bulk Containers with material either based on volume or weight. In the case of gravimetric filling machines, the process is controlled such that the containers are filled with a fixed weight of bulk product. Although the system consists of a single feeder, such as the one shown in Figure 1.6, handling a single material, the machine design can be very complex in order to achieve accurate weighing. The measured weight may be the net weight (only the weight of the material) or the gross weight (overall weight of the container and the material). Thus, these machines can be further sub-categorized into net weighers and gross weighers.

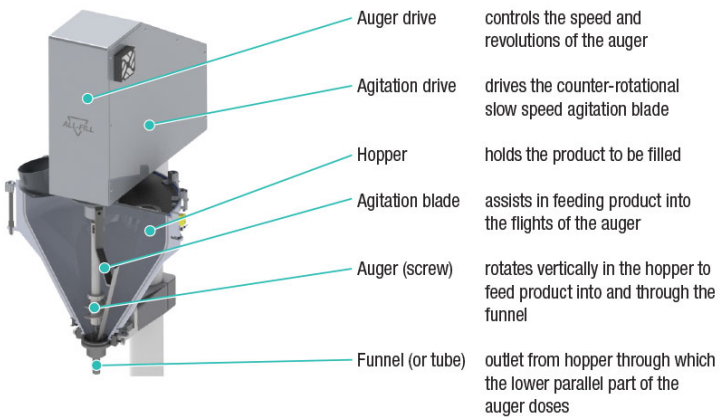

Figure 1.6: Gravitational Filling Machine Feeder [11].

2. **Discrete Totalizing Weighers.**

   As the name indicates, this single feeder category encompasses machines that add up discrete batch weights. Summing up the results will yield an accumulated overall weight of material, which can be very large (up to 10 tons in some applications). The throughput can be recorded as well.

   (a) **Shipping and Receiving Weighers**.

   When shipping and receiving bulk material, it is useful to weigh the material being transferred between a silo and a vessel, for example, when grains are unloaded from ships in ports. The vessels may be as large as a road/rail tanker, barge, or a ship. As a result, this is a suitable application for discrete totalizing weighers due to the large amount at hand, and since the material has to be gradually transferred even if there's no need for weighing. The machine, shown in Figure 1.7, consists of three hoppers - the top surge hopper, the central weigh hopper, and the bottom discharge (or surge) hopper. The top hopper continuously feeds material to the central one where weighing occurs. Once a discrete load is weighed, the content is emptied into the bottom hopper, which in turn delivers the discrete loads to the bulk. Similar to the top hopper, the flow out of the bottom hopper is continuous as well.

Figure 1.7: Material Totalizing Batch Weigher [12].

(b) **In-Process Weighers.**
Similar to shipping and receiving weighers, these weighers determine cumulative weights of a product stream. However, the difference is that they are primarily used within manufacturing processes such as grain and rice milling. Due to the nature of the application, the weighing capacity is typically smaller as well. They also consist of a three-section hopper system similar to that in Figure 1.7, except that it is in a more compact integral form. They allow the quantification of milling efficiency while maintaining a smooth and continuous process flow.

3. **In-Motion Weighing Systems.**

In this type of system, measurands that may be continuous or discrete are weighed while in motion. The goal is to determine mass while maintaining minimal interference with the flow of the measurands.

(a) **Continuous Weighing Systems.**

Particulate material, such as gravel, salt and cement, often flow in continuous streams in automated processes. This class of systems can determine the mass flow rate of material using a combination of mass and velocity sensors and, as a result, the total mass of the delivered or transferred material can be calculated. This is because the mass flow rate can be obtained by multiplying the measured mass by the belt speed and dividing it by the length of the weighing platform. For example, belt weighers are continuous weighing systems that are generally constructed by mounting weigh frames on load cells which are in turn mounted on support structures. The weigh frames include idler rollers that facilitate the motion of the conveyor belt they carry. Bulk material to be measured during the motion sits on top of the belt. A device such as a tachometer can measure the belt speed. Figures 1.8, 1.9 and 1.10 illustrate the construction of the described system. Other examples of continuous weighers include impact weighers, curved plates, and Coriolis force mass flow meters.

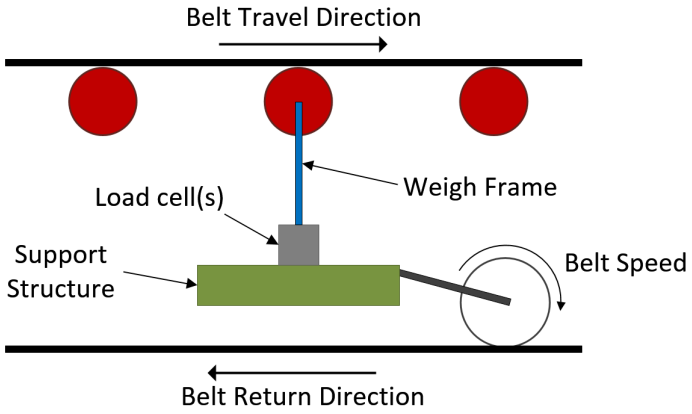

Figure 1.8: Schematic Representation of a Belt Weigher.

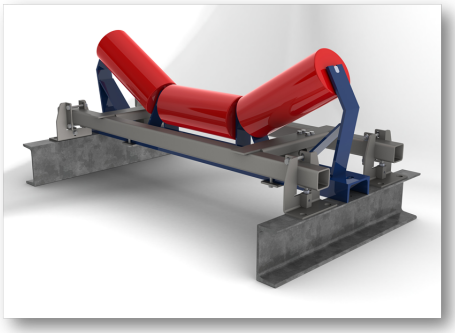

Figure 1.9: Roller supported by Weigh Frame [13].
© Ametech Systems Pvt Ltd.

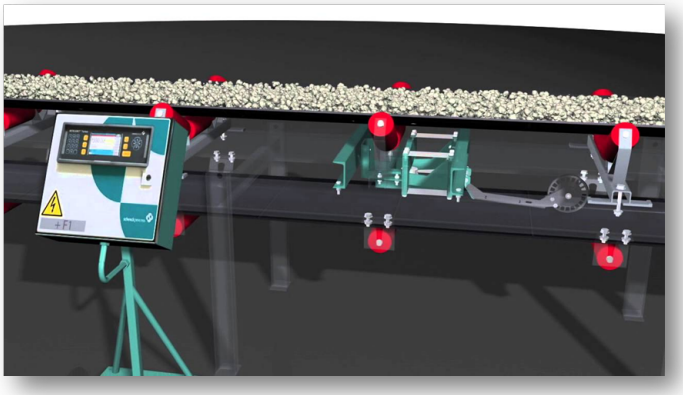

Figure 1.10: Continuous Belt Weigher [14].
© 2016 Schenck Process Holding GmbH.

(b) **Discrete Mass Weighing Systems.**
These weighers can capture mass measurement of discrete items as they pass over the weighing platform. A total weight can be calculated depending on the application, such as in road vehicle weighing; a weighing platform (weighbridge) can measure the loads on each wheel or axle of the vehicle and sum the data to determine the overall weight. This type of application is commonly referred to as weigh-in-motion and Figure 1.11 shows one implementation of the system. Similarly, the mass of a moving locomotive, and its individual wagons if desired, can be measured using rail weighbridges.

Figure 1.11: Road Vehicle Weigh-In-Motion [15].
© 2016 Intercomp.

Another important class of discrete mass weighing systems is catchweighers or checkweighers. A catchweigher is a device that senses the mass of individual packages moving on conveyor systems. The belt type checkweigher, shown in Figures 1.2 and 1.12a, works similarly but with the feature of verifying that the package weights are within prescribed limits. The subcategory of catch and check weighers is particularly important in this thesis since they are the closest to the weighing system we developed. However, since they are defined as machines that weigh packages individually, our weighing system cannot be necessarily considered to belong to this category.

The classic low-pass filter is often insufficient for filtering sensor noise in checkweigher systems. This is due to an existing trade-off between accuracy and time delay/speed when choosing the cut-off frequency f_c. The typical ideal weighing cycle of the weigher is shown in Figure 1.12b. The weighing time t_w is of importance especially in high-speed high-accuracy weighing. When f_c is decreased, measurement accuracy improves at the expense of a longer settling time. This delay (equal to the settling time) can result in a missed weighing cycle if its length exceeds t_w. On the other hand, a higher f_c will perform faster but result in greater oscillations increasing measurement error. This fundamental limitation of the filter is shown in Figure 1.13. An overview of the

numerous publications that attempt to overcome this limitation is provided in the following section.

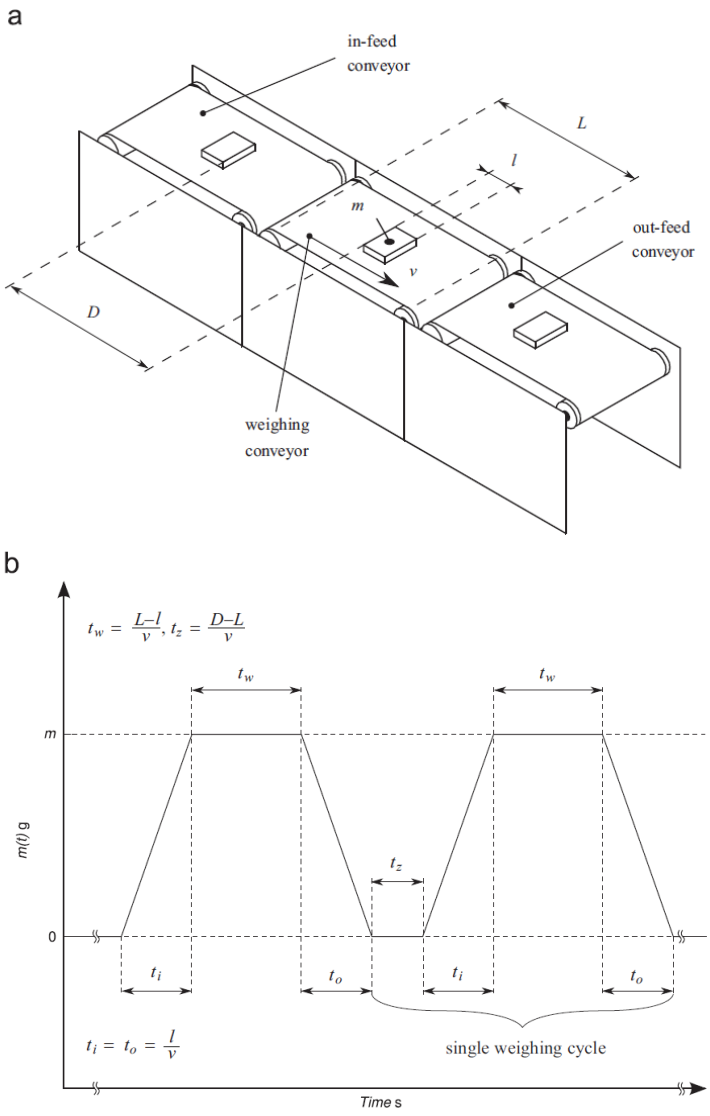

Figure 1.12: A conveyor belt type check weigher and its ideal weighing cycle. L is the length of the weighing conveyor, l and m denote respectively the active length and the mass of the weighed object, D is the distance between two consecutive objects,and v denotes the belt speed. (a) A conveyor belt type checkweigher. (b) Weighing cycle of a conveyor belt type check weigher [16].

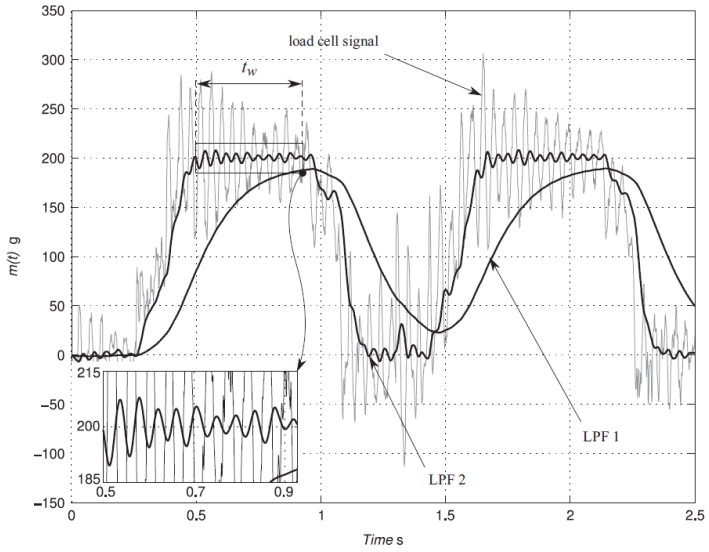

Figure 1.13: Varying the passband of a low-pass filter results in a tradeoff between measurement accuracy and settling time [16].

1.3 Related Work

Achieving accurate mass readings in a noisy and fast-paced environment is a crucial consideration when designing weighing systems. As a result, different filtering techniques and approaches have been proposed in literature. This chapter provides an overview of such filters designed for catch/check weighers and/or belt platform scales. As mentioned in Section 1.2, the machine described in this thesis is closest to the catchweigher category. In the first subsection, model-based estimation methods are presented and analysed. In these methods, a catchweighing system is modelled and an estimate of the weight of objects moving on its belt is calculated based on that model. The second subsection discusses techniques that involve a control loop, which provides a mass measurement while dynamically compensating for displacement caused by the change of weight. The final subsection covers different filtering techniques from the signal processing field commonly implemented to filter load cell signals.

1.3.1 Model-based Estimation Approaches

Since Rudolf E. Kálmán published his famous paper in 1960 [17], a variety of applications incorporating the Kalman filter have emerged. Model based mass estimation using load cell readings is one such example. Various publications, [16, 18–27], have adopted the mass-spring-damper model, shown in Figure 1.14, as an effective model of the load cell dynamics and sometimes even as that of the entire checkweigher. Note that the system is time-variant since the load $w_{(t)}$ varies with time.

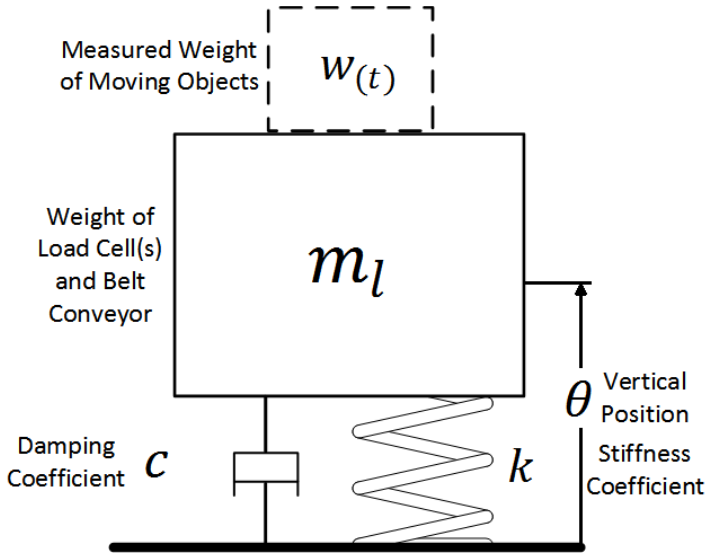

Figure 1.14: Mass-Spring-Damper Model of a Check Weigher.

Based on the mass-spring-damper model, the Kalman filter can be used to estimate the steady state value of load cell measurements and, as a result, the weight of the measured object. Early work by Ono et al. [18] proposes such an approach in an attempt to improve weighing performance. The main metrics for performance, common in the literature, are weighing accuracy and weighing time (or speed). Low measurement error and high weighing speeds are desired and there exists a trade-off between the two. The paper derives a lower bound for weighing time based on conventional static weighing, where the measurand lies statically on a scale to be weighed. Then, the mass is estimated with two methods:

1. State estimation algorithm using the Kalman filter for a linear system model. This assumes that the mass of the measurand is very small compared to that of the scale pan to achieve a linear model. The estimation can be done in real-time.

2. Extended Kalman filter (truncated second-order filter) for the time-variant system model. At the time of writing of the paper, data processing could not be done in real-time.

While the method was successful experimentally, the scale in the setup is not realistic or practical compared to conventional scales. It consisted of a magnetic damper, weigh spring, differential transformer and a scale-pan, which ensures that it closely represents a mass-spring-damper model. The proposed method may or may not work with common scales.

In [19], Tariq, Balachandran and Song model all the dynamical subsystems of a modern checkweigher in an attempt to better understand the dynamics of the system and improve performance as a result. For the weighing sensor, the same mass-spring-damper model as discussed above is proposed. However, $w_{(t)}$ is analysed in greater detail and three different functions are evaluated to represent $w_{(t)}$. More complex models are formulated for packages and for the conveyor transport subsystem. When comparing the simulation results of the model to the experimental results, the proposed modelling offered improvements over other existing models. Nevertheless, there were limitations that may have arisen from the lack of comprehensive understanding of the geometry of the mechanical subsystem. Although the work is beneficial when designing the components of a checkweigher, there is little control over the dynamics of the moving packages. Signal processing based approaches may provide similar or better weighing performance at a lower level of design complexity as we will discuss.

Balachandran later proposed, with Halimic in [20], a Kalman filter approach based on the weighing sensor model described in his previous work with Tariq and Song [19]. The experimental results suggest that the method is an effective alternative to conventional filtering methods particularly when the low frequency noise overlaps with the bandwidth of the useful sensor signal and when non-linearities exist in the system.

McGuinness et al. [22] addressed such concerns in one interesting case study on modelling the physics in a high-speed application. The system under consideration is a fruit weighing system for the purpose of sorting. The initial observation was that higher than desired measurement errors were detected for shorter weighing cycles and heavier fruit. They hypothesized that low frequency noise contaminated sensor data and could not be effectively filtered out with low-pass filters as a result. The authors examined the power spectra of unfiltered load cell data at different speeds and weights to identify the sources of noise. One of the major high frequency noise sources turned out to be sound as verified by inducing sound in the system and recording it. One or two more concerning lower frequencies, inversely proportional to fruit mass, were detected as well. This was inconsistent

with a simple harmonic oscillator model. As a result, they augmented this up and down model with a side to side rocking motion model to represent the sideways motion between the two load cells carrying the fruit. Based on their mathematical model and experimental data, they believe that the new model accounts for the lower noise frequencies. In the end, they still did not recommend a model-based approach but rather considered mechanical design changes and adaptive filtering techniques. Unfortunately, the work did not attempt to implement the solutions and so the evaluation of the propositions was not done.

Another paper by Boschetti et al. [25] suggests a model-based approach for a particular multi-head weighing system design. The problem, again, was that a simple low-pass filter implemented on the output of the load cells did provide sufficient performance due to low frequency vibrations. A load cell functions by measuring mechanical displacement through one or more strain gauge(s) embedded in a certain type of material. The strain gauge(s) are placed in a Wheatstone bridge circuit which produces a change in voltage when their resistance changes as a result of strain/force. Although the voltage is measured due to the convenience, strain and mass can each be obtained by simply multiplying the voltage with a corresponding constant. The proposed model-based approach was to dynamically estimate and compensate for environmental vibrations after measuring different housing accelerations of the system. The acceleration measurements can be input into a dynamic model to produce an estimate of strain caused by vibration in the load cell response. This estimate can then be subtracted from load cell readings to reduce vibration and then the resulting signal is further processed by a low-pass filter. The method was experimentally verified to be effective.

In the end, different weighing sensor and weighing machine designs will have different properties in terms of modelling and the frequencies of noise and meaningful sensor signal. There is always the question of whether a simple harmonic oscillator model is accurate enough to outperform other filtering techniques and, if not, whether identifying a better model is worth the effort. In other words, a model-based estimation approach can work well for some systems and perform similar or better than other approaches. However, that may not always be the case if the system model needs further development. In that scenario, alternative approaches may offer comparable results at a lower complexity compared to advanced model based approaches. Also, model-based approaches tend to be less robust to the different levels and sources of noise.

1.3.2 Control-based Approaches

For certain types of weighing sensors and systems, it is possible to formulate a control scheme based on a system model, such as those presented in [26] and [27]. The role

of the control system is to electrodynamically compensate for certain sources of noise. A common class of such sensors is electromagnetic force restoration (or compensation) load cells, abbreviated as EMFR (or EMFC). An EMFR sensor charges an inductive coil, floating the scale bed in an electromagnetic field via a lever arm (or balance beam). Weight variance causes the movement of a ferrous material through that coil creating a fluctuation in the coil current proportional to the weight of the object. This movement is detected by a position sensor such as an optical one. The main feature of EMFR technology is to actively suppress any mechanical noise through high-speed (> 1 kHz) feedback control. As a result, the force created by the measurand can be calculated from the sensed coil current with minimal (a few *nms*) mechanical movement occurring in the system. It is also possible to measure low forces in the horizontal direction as proposed in [28], although it is of little interest for weighing applications but rather for force measurement. Figure 1.15 shows the block diagram of the EMFR sensor.

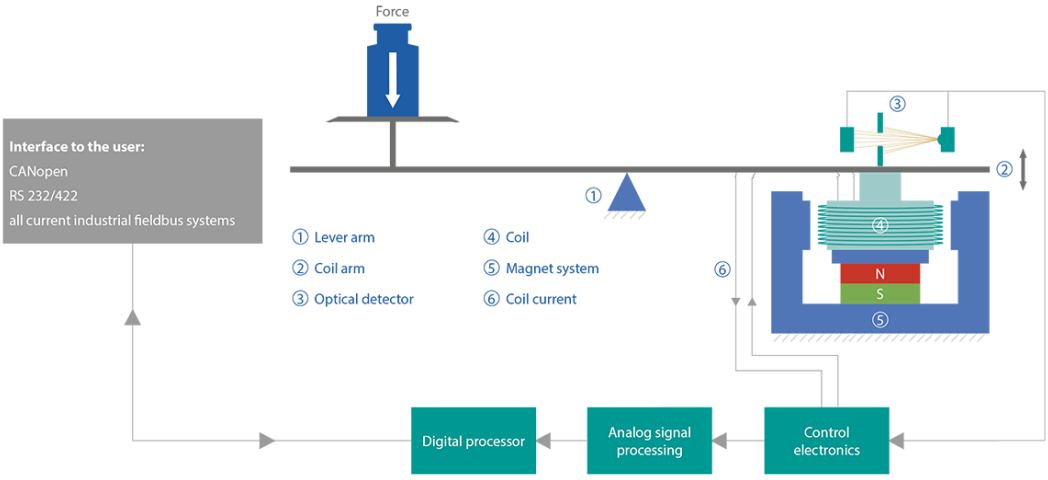

Figure 1.15: An example diagram of an EMFR sensor [29].
© 2015 Wipotec Wiege- und Positioniersysteme GmbH.

The control system design approach has attracted interest in the research literature since it uses modern control theory to improve the sensor system. Halimic et al., for example, propose performance improvements of dynamic weighing systems using a Linear Quadratic Gaussian (LQG) controller rather than the classic PID controller in [21].

Maier and Schmidt proposed an integrated digital control and filtering system for a high resolution EMFC scale in [30]. In addition to describing the concept and discussing major

problems of the hardware and software design, they also present an intelligent multi-filter scheme similar to techniques that we will discuss in the next subsection. The unique aspect of the system compared to the one shown in Figure 1.15 is that it requires neither a high resolution analog-to-digital converter (ADC) nor an additional analog filter; they replaced the analog realizations with digital ones. The paper overcomes slow low-pass filter transient response by switching between three different filters based on steady-state criteria. This is done by switching to a moving average Finite Impulse Response (FIR) low-pass filter with a relatively low cut-off frequency, MAF 1, when the weighing signal is steady. As the weight begins to change, another MAF with a higher cut-off frequency, referred to as MAF 2, filters the signal instead. A simplified Kalman filter is utilized during the switch to maintain continuous output signals.

The issue with EMFR technology is that it is more expensive than both standard and enhanced load-cell scales. Thus, it has been more common in laboratory equipment due to its high cost, vulnerability to damage and low capacity [31]. However, recently this technology has been implemented in certain industrial applications offering relatively more cost effective solutions, better ruggedness and capacity. Examples of industrial EMFR sensor suppliers include Mettler-Toledo in the US and WIPOTEC in Europe. Both companies use the EMFR technology for the high performance checkweighers.

Another interesting technology is the SAW (Surface Acoustic Wave) sensor technology, commonly used for weighing electronic components when used in weighing applications [32]. SAW sensors are a class of micro-electro-mechanical systems (MEMS) which rely on the modulation of surface acoustic waves to sense a physical phenomenon. The sensor transduces an input electrical signal into a mechanical wave which, unlike an electrical signal, can be easily influenced by physical phenomena, such as displacement due to weight. The device then transduces this wave back into an electrical signal. Changes in amplitude, phase, frequency, or time-delay between the input and output electrical signals can be used to measure mass. The accumulation of mass on the surface of an acoustic wave sensor will affect the surface acoustic wave as it travels across the delay line. The velocity v of a wave traveling through a solid is proportional to the square root of the product of the Young's modulus E and the density ρ of the material. Compared to EMFR, SAW sensors have a better capacity and a similar level accuracy. Unfortunately, their presence in the weighing industry and market remains limited.

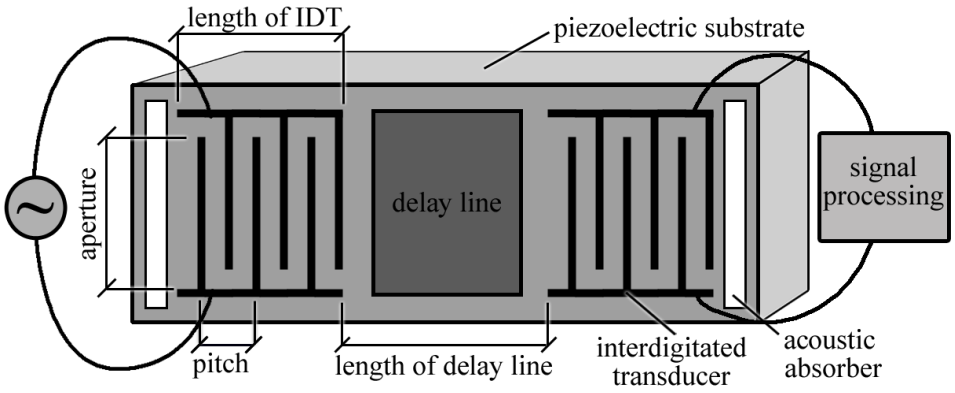

Figure 1.16: Surface Acoustic Wave sensor interdigitated transducer diagram [33].

1.3.3 Advanced Signal Processing Filtering Techniques

In a fashion similar to [30], several advanced filtering techniques were proposed in the literature often mixing different filters and/or switching between them, using adaptive or time-variant filters, and/or combining/cascading some of the identification-based, control-based, and advanced signal processing techniques to yield better dynamic weighing performance.

In [34], Halimic et al. propose an adaptive deconvolution filter cascaded with an additional noise filter. The adaptive filter suppresses noise within the bandwidth of the desired signal with the side effect of amplifying signals outside the bandwidth. The noise filter counters this disadvantage and the performance is significantly enhanced compared to processing done in a checkweigher designed by Loma Systems. Later in [23], Halimic et al. devise another signal processing approach combining Fuzzy Logic and Artificial Neural Networks. The method proposed improves upon Jang's Adaptive Network based Fuzzy Interference System (ANFIS) [35] by introducing a systematic approach for deciding the number and initial shape of the membership functions. However, this initial setting needs to be modified for each measurand since it depends on its characteristics. Compared to cascaded filters and Loma Systems processing, the approach yields better weighing accuracy and throughput.

Many other papers propose adaptive techniques, also common in industry, such as [36]. Umemoto et al. combine an adaptive notch filter with the simple moving average method yielding better accuracy for continuous check weigher mass measurement.

Another class of effective dynamic weighing filters, time variant filters, can be seen in the works [24], [37], [16] and [38]. The underlying principle here is to overcome the fundamental

limitation of low-pass filters, shown in Figure 1.13 and described in Section 1.2, by varying the cut-off frequency. Unlike the technique of switching between two cut-off frequencies proposed in [30], this is implemented by varying the bandwidth f_c as a function of time. When the weighing cycle begins, which is detected by photocells, the low-pass filter has a high f_c in order to decrease the time delay (settling time). This f_c decays exponentially as a function of time and settles to a fixed value allowing a high accuracy measurement in the steady state portion of the weighing cycle. In [24], this is done in simulation with continuous time low-pass Bessel filters. Pietrzak further expands this idea in [37] and [16] by using Infinite Impulse Response (IIR) filters, also used in [39]. The IIR filters are cascaded and designed in discrete time. The results are validated experimentally and indeed yield improved dynamic weighing performance compared to an identification-based approach, time-invariant Bessel and time-invariant critically damped filters. Pawlowski et al. confirmed that the proposed technique is effective when implemented on a practical system in [38].

To summarize, signal processing filtering techniques have the advantage of being independent of the system model at hand offering simplicity at the expense of more extensive tuning. They can be more robust to different sources and magnitudes of vibrations and noise. They also can be applied to the output of different force sensor types overcoming the limitations of certain sensors. For example, EMFR sensors used in control-based approaches have a limited weighing capacity which is not practical for some applications.

As a result, we will adopt the filtering approach by Pietrzak et al. [16] in this work for reasons that will become evident when we describe our prototype. There are some similarities in our work to the multi-stage conveyor belt weighing idea presented in [40] as well. Tasaki et al. presented a new weighing scale consisting of multiple belt conveyors placed in a sequence along the direction of motion of packages. They designed a digital FIR filter and a filtering algorithm to achieve good results at a reasonable accuracy. However, the weighed objects were singulated on the weighing platform and had to be spaced within a specified range to be correctly weighed. This is because high-accuracy high-speed weighing for non-spaced items does not seem feasible with existing technologies without creating some space.

It is worth noting that combining identification-based approaches with advanced signal processing techniques can also yield fast, accurate and robust results as shown in a recent paper by Niedźwiecki et al. [41].

1.4 Outline of Thesis

Design concepts that address the problem at hand are presented in Chapter 2. The chapter continues to describe the first small scale proof of concept for the selected design, and subsequently the full scale prototype design. Chapter 3 details the different filtering techniques that are implemented in experimental verification. Later in chapter 4, the experiments conducted and their results are summarized. Some important notes regarding zero adjustment and calibration typically done for scales are made. In addition, spacing requirements are discussed. Finally, Chapter 5 describes the conclusions, and outlines directions for future work.

Chapter 2

Weighing System Design

The main problem addressed in this thesis is to provide a realistic assessment of the individual weights of packages moving along a conveyor in a relatively non-singulated and non-spaced fashion. The target conveyor speed is 0.2 m/s and the maximum average error is 0.02% of the weighing capacity. Design concepts are formulated, an initial basic proof-of-concept prototype is built and evaluated, and a larger scale prototype is designed including parts and interface selection.

2.1 Design Concepts

The following criteria can be considered when assessing a design:

- Responsiveness/throughput (*packages/seconds*) - A measure of how many packages can be weighed per second.
- Sensor Error ($\%$) - A measure of the difference between the true mass and the actual sensor measurement, for a given system speed.
- Cost ($\$$) - A measure of the total cost of the design.
- Maximum Weight (kg) - A measure of the maximum weight that can be detected/tolerated without damage.
- Component Integration ($\%$) - A measure of the how easy it is to assemble and maintain the technologies selected for the design. A more simplified design with all components integrated within one package is desired.

- Product life (*days, months*) - How long it lasts before needing a replacement.
- Size (L) - A measure of the volume taken up by the transducer.
- Power Consumption (*watts*) - Amount of power the system consumes.

Within the scope and duration of this thesis, three main criteria were considered among these: cost, accuracy and responsiveness.

After brainstorming, the following three designs concepts were chosen for a potential device:

1. **Pick and Place Weighing Robotic Manipulator** An interesting approach is to have a pick and place robotic manipulator picking up items moving on the conveyor system. The system, in Figure 2.1, can then weigh them using load sensors in the arm and place them back on the line. An idea that somewhat resembles this concept was implemented by Tariq and Balachandran in [42] by replacing the weighing belt stage in a checkweigher with an intelligent robotic arm and a static scale. The arm would pick a package from an in-feed conveyor, place it on the scale, and then place it back on the out-feed conveyor. They were able to sort the products while maintaining the same throughput as the original check weighing system. The main concern with the concept is that it can be difficult to select or create a cost effective robotic arm that can pick up items of different shapes and sizes present in a sorting facility.

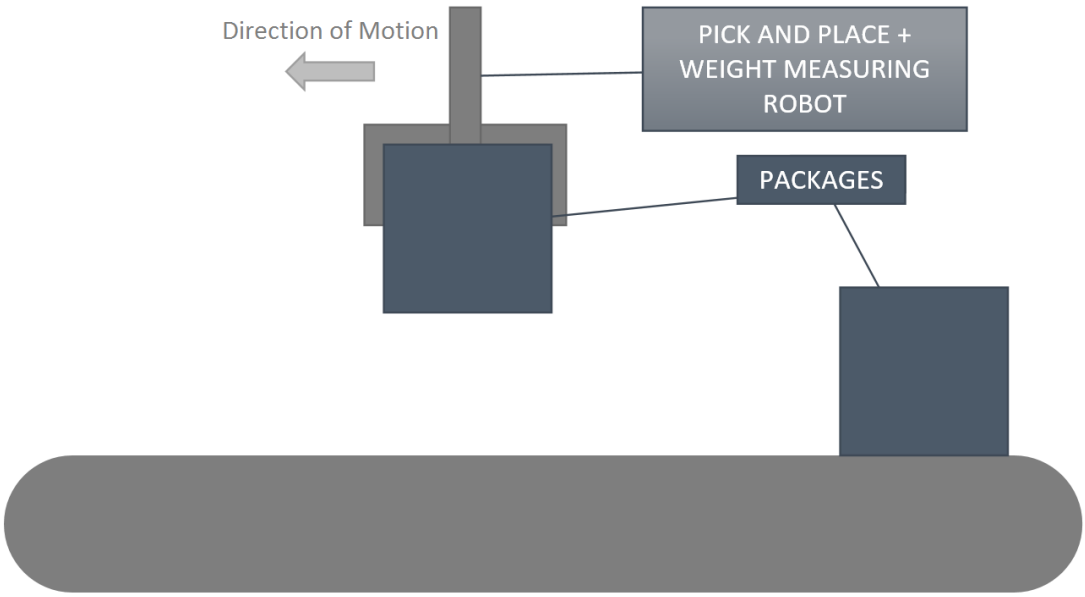

Figure 2.1: A robotic manipulator picks up packages from a moving belt conveyor to weigh them.

2. **Embedded Weight Sensing Grid** The second design concept consists of a grid of smaller stand-alone scales placed under a conveyor system as shown in Figure 2.2. One way to implement such a concept is by using thin film force/load sensing units in a grid format and adding compliant material [43] to ensure good contact between the packages and the sensors. Figure 2.3 illustrates the concept. Unfortunately, available force sensing resistors are known to have low accuracy and are not recommended for weight measuring applications. Using a different type of sensor can increase cost and complexity on the other hand.

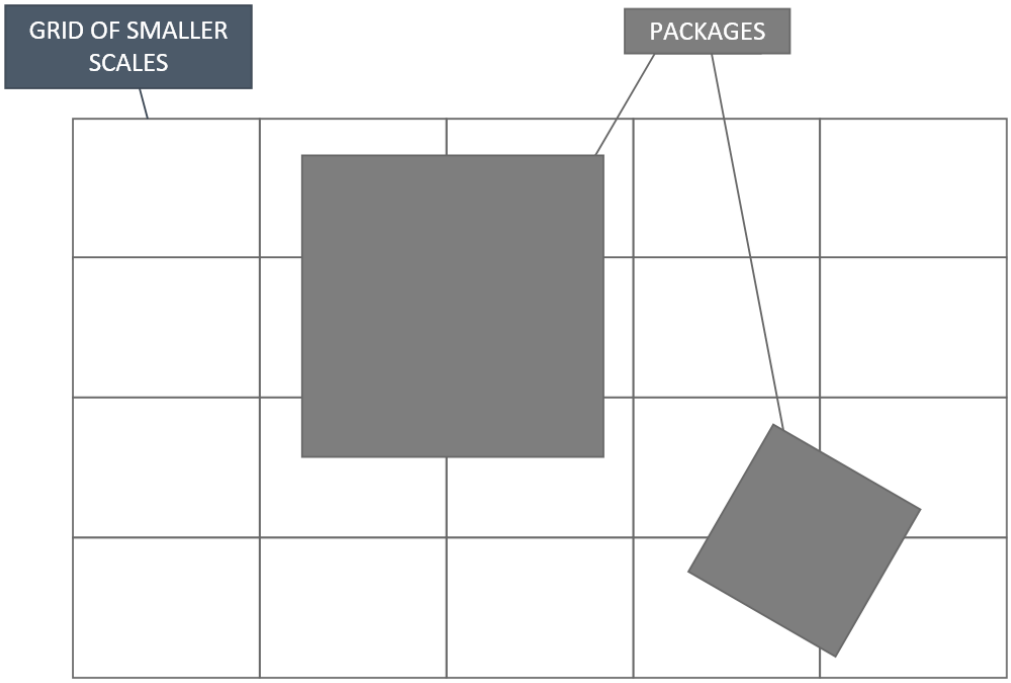

Figure 2.2: Grid of force sensors.

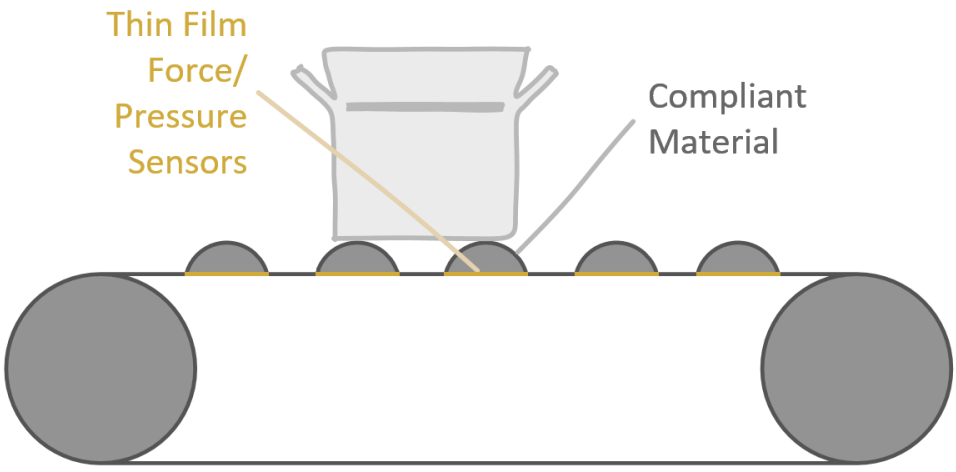

Figure 2.3: Concept 1: Thin film pressure sensor embedded in compliant material grid.

3. **Grid of Scales** Another implementation of the idea in Figure 2.2 is to mount a conveying system such as rollers or conveyor belts on a weight sensor such as load cells. The concept, shown in Figure 2.5, resembles a skate wheel conveyor and consists of passive rollers attached to load cells (as illustrated in Figure 2.4), or another weight sensing device if desired. The sensors will remain static as packages roll on the conveyor as opposed to the sensors in concept 2. Using a vision system, it is possible to locate packages and rollers, and calculate the weight of the packages from the load cell measurements. The conveyor may consist of a grid of load cells and may have a sloped surface to allow packages to move, which is a disadvantage in terms of speed and cost. It is possible to actuate the conveyor at the expense of complexity and additional cost. Another option is to use belt conveyors. Expected issues include: belt tension, friction between belt and grid surface, possible high cost, and error due to overlapping packages. The issue of overlapping packages will require some spacing between items to minimize errors.

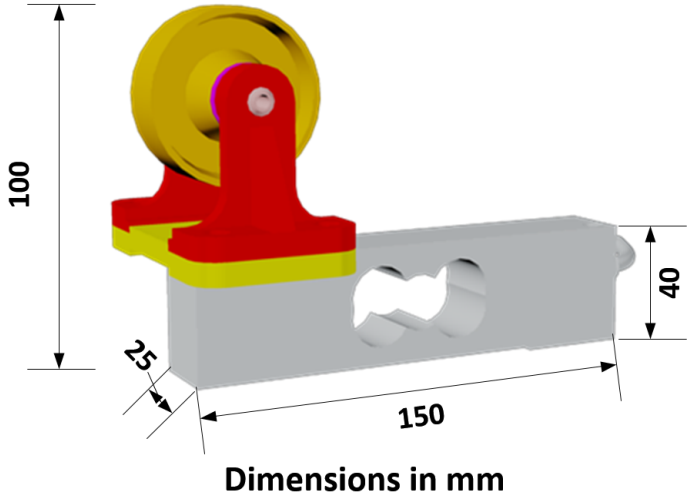

Figure 2.4: Weight Measuring Roller.

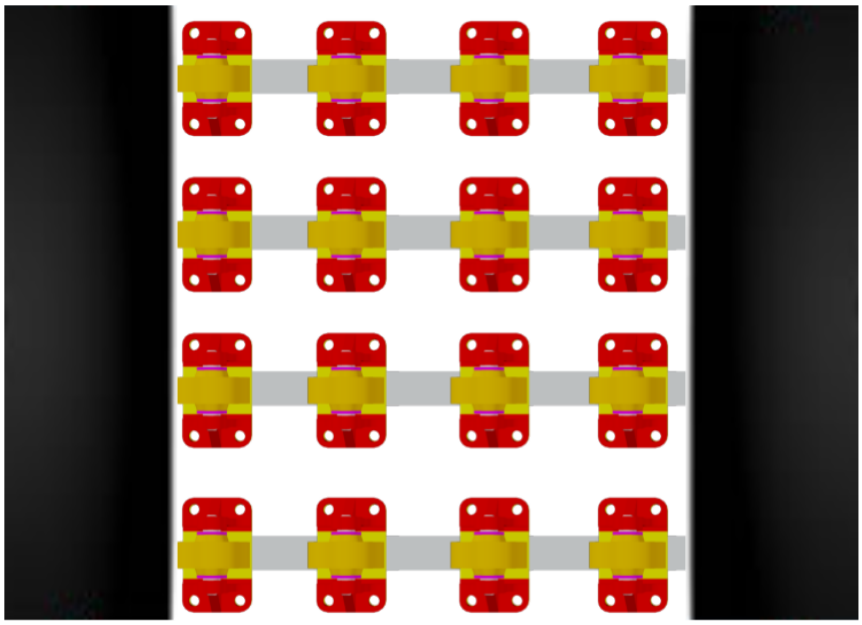

Figure 2.5: Concept 3: Array of Weighing Rollers between Belts.

4. **Single Row of Scales** A potential simplification of the third design is to replace the sensor grid with a row of sensors placed between the belt conveyors as shown in the Figures 2.6 and 2.7. This will reduce the cost and allow a smoother package flow. However, an advanced technique is needed to estimate the weight of the packages based on the sensor measurements, which may or may not be very accurate. This technique may require some mathematical formulation to estimate mass and may be similar to that used for truck weigh in motion (WIM) systems.

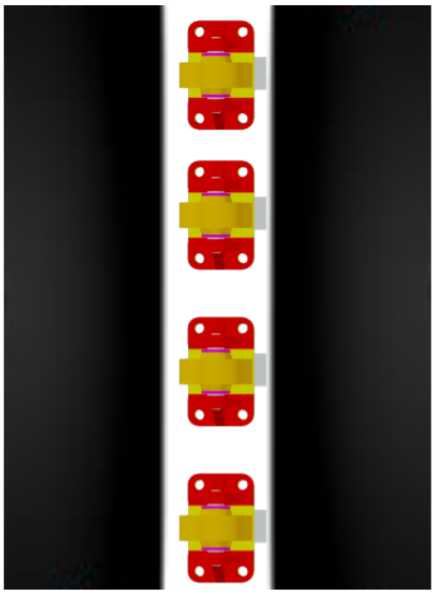

Figure 2.6: Concept 4: Single row of weighing rollers between belts top view.

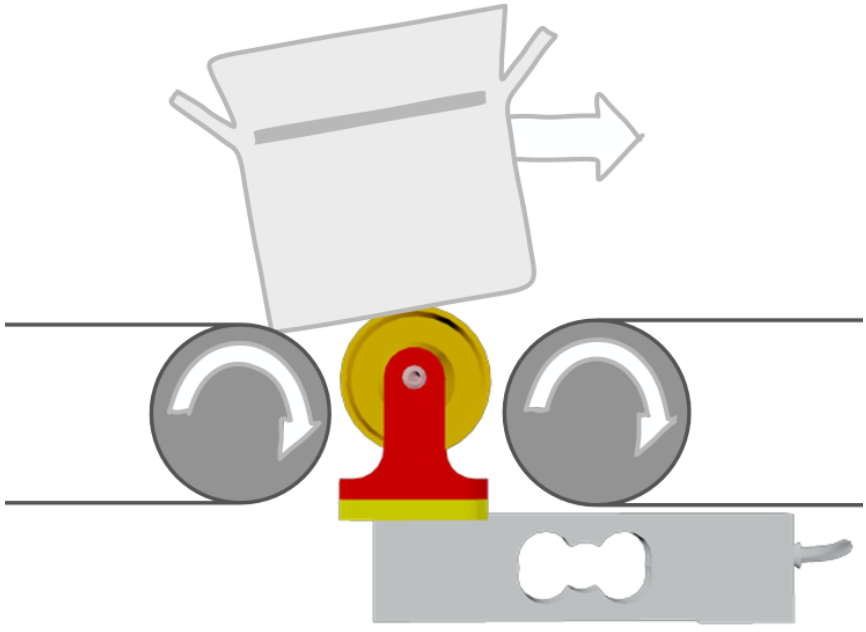

Figure 2.7: Concept 4: single row of weighing rollers - side view.

Among the above four design concepts, the third idea was selected for the proof-of-concept. The rationale is that the first concept will be difficult and costly to implement, the second concept will not be sufficiently accurate, and the fourth concept will require more spacing equipment compared to the third.

2.2 Small Scale Proof of Concept

2.2.1 Prototype Development

Sensors and Instrumentation

The most important component for the selected design is the load cell/transducer. Several products from companies such as HBM, Scaime, LoadStar, Futek and Ricelake were considered. The selection approach involved looking for manufacturers, finding products designed for dynamic weighing applications, and then evaluating based on accuracy and price.

AG series single point load cells, Figure 2.8, with an eNod3-C controller, Figure 2.9, were selected. The aluminum built AG series model is small in size, available in C6 class accuracy which is used in checkweighers, and is designed for dynamic weighing applications. The classification is defined as C6 per the OIML R 60 recommendation by the Organisation Internationale de Métrologie Légale (OIML). The recommendation provides in detail the requirements for the certification. It is sufficient to pick a load cell class based on the application; C3 and C6 are sufficient for checkweighers with C6 being more accurate than C3 [44]. The AG load cell has a capacity of up to 100 kg and costs around $95. Load cells with similar accuracies from different manufacturers are mostly in the $200-$400 range. Load cells that are cheaper, such as the $7 CZL635 model from Phidgets, have much lower accuracies, around 15% error for CZL635.

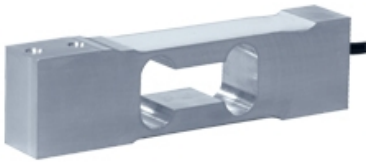

Figure 2.8: Scaime AG series load cell [45].
© Scaime

The eNod3-C controller has built-in voltage amplifiers, signal conditioning and analog to digital converters to facilitate high speed weight measurement. It has RS232/RS485 and CANbus outputs; the latter allows real-time analysis of the output. It costs around $325.

Figure 2.9: Scaime eNod3-C load cell controller [46].
© Scaime

Platform Construction

The prototype during the construction phase is shown in Figure 2.10. The fixed ends of the load cells are attached to a rectangular Plexiglass sheet with two bolts for each cell. The sheet sits on four pieces of wood for stability. On each cell, a small piece of hard plastic is attached with two bolts and a few nuts. The nuts are used to create space between the plastic and the cell in addition to keeping the bolt in place. A rolling wheel assembly is attached to each small piece of plastic. This way, all the force will be transferred to the load cell through the two bolts on the loading end for proper measurement. The resulting system is shown in the first image of the Figure. Next, a tabletop is made to sit above this system without touching it. Three holes are made on the tabletop's surface so that an object moving on the tabletop can make contact with the wheels. In preliminary experiments, a box can be manually pushed on the surface of the table, making contact with the wheels, in an attempt to measure its weight. More and/or different types of wheels can be attached for a different setup. Also, the entire setup can be placed on an incline causing the box to slide due to gravity.

A slippery surface is added to allow the package to easily slide as shown in the images in Figure 2.11. The dimensions of the overall prototype are $90cm$ x $33cm$ x $16cm$ while those of the test package are $23.3cm$ x $18.9cm$ x $11.3cm$.

The setup can be placed on a $34cm$ high stand creating a 23.5 *degrees* incline as shown in Figure 2.12.

Figure 2.10: Photos of prototype construction.

Figure 2.11: Photos of the assembled prototype.

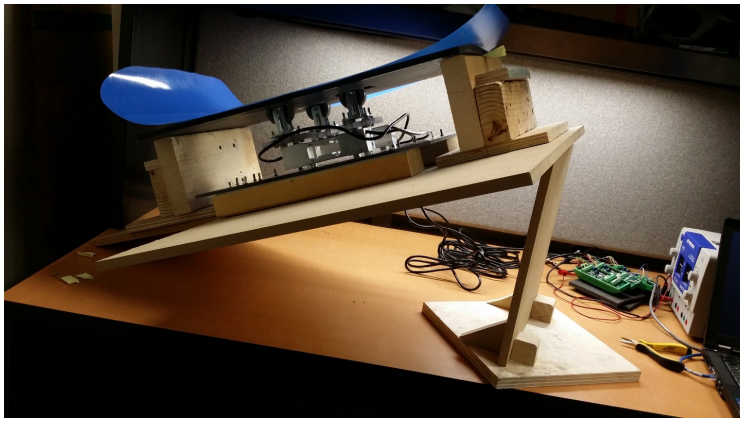

Figure 2.12: Prototype placed on an incline to allow packages to slide freely.

Interface

The second step involves connecting each AG-10 load cells to the eNod3-C controllers and interfacing via Scaime's eNodView software. The limitation of the software however is that it does not collect data from multiple controllers in real time. As a result, a LabVIEW program was created for data acquisition via CANbus and CANOpen protocol. The eNodView program is useful to easily configure the controllers and save the configuration settings in their memory. It allows communication through a serial COM port (RS232 9-pin connector) with the Fast SCMBus protocol (as well as other protocols). Fast SCMBus can run at a maximum speed of 115200 *bauds* or *bits per second*. The CAN bus protocol is faster with a maximum of 1 *megabaud*. Using eNodView, the load cells are calibrated using either a theoretical or a physical calibration method. The theoretical method involves inputting the sensor sensitivity and capacity to eNodView, while the physical one involves loading the cell with 3 known static loads and inputting their corresponding expected readings. Then, the scale is adjusted to have a reading of zero in the no-load state. These steps were completed and after some tuning of other parameters, static weighing of objects of known mass was done successfully. Figure 2.13 is a screenshot of the output when two different known masses (1469 *grams* and 879 *grams*) are weighed. The amplitude on the y-axis is in *grams* x10.

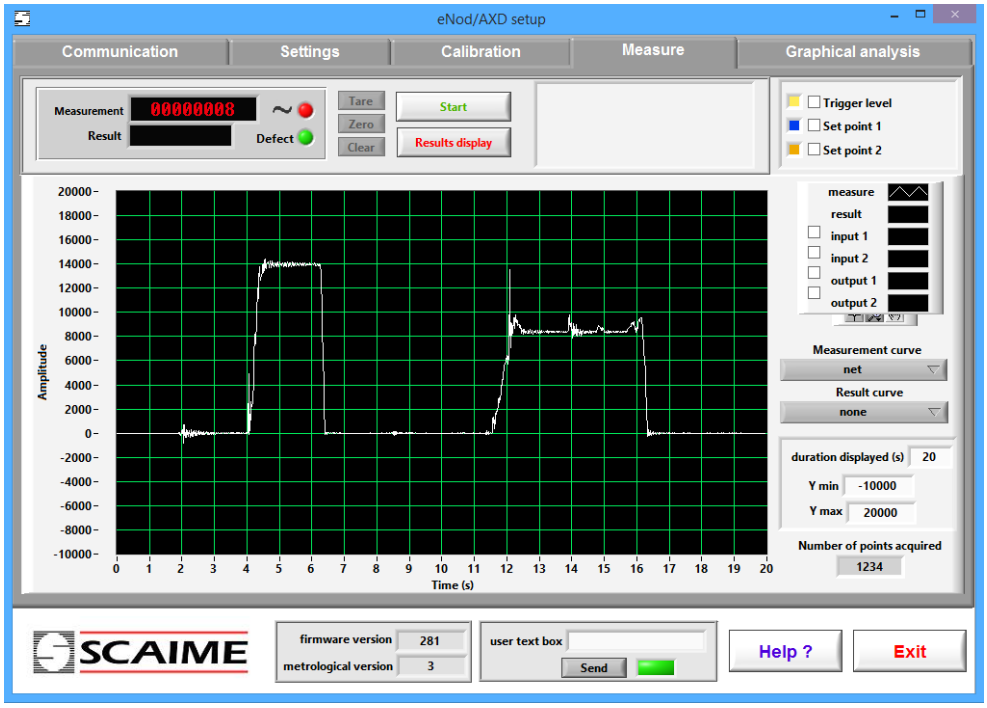

Figure 2.13: Screenshot of eNodView software.

The software also allows the activation and tuning of additional filters for graphical analysis: A/D converter filter (control *measurements/sec*), digital low-pass filter (filter type, order, frequencies, and coefficients), digital band-stop filter (cut-off frequencies and coefficients), and a self-adaptive filter. It also has a checkweigher mode in which the average value, number of complete cycles and other useful information can be provided. To benefit from the eNodView software and receive real time data, it is best to configure and analyse data for individual load cells using serial communication. Once this is done, the configuration can be saved, and CAN bus can be used to monitor the network of controllers/load cells in real-time using LabVIEW. The CAN connection can be made as illustrated in Figure 2.14 where each node is a controller. The bus consists of two lines a high, CAN H, and a low, CAN L, with two termination resistors at each end. Each of the nodes connects to the corresponding line. The eNod3 controllers are connected as slave nodes and communicate with a master node, which is a machine running the eNodView of LabVIEW software.

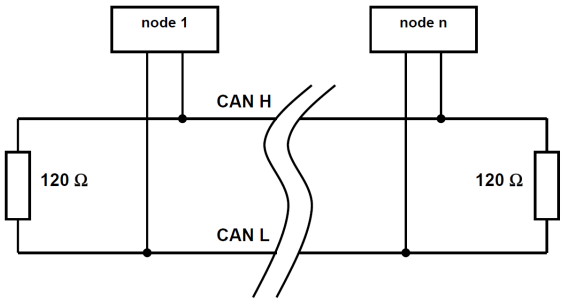

Figure 2.14: CAN bus connections.

2.2.2 Experimental Results

In this experiment, a box with three different masses slides on the surface making contact with one roller (Roller 1) first and the other two (Rollers 2 and 3) after that. Mechanical vibrations were observed in the system which can be attributed to the wheel's eccentricity and the load cells' natural response to the force applied on one end. These vibrations can be observed visually during the experiment. Also, when the wheel is left to rotate without applying a load, it produces vibration. Using a 4th order Bessel filter, which acts as a low pass filter, it was possible to get a 'cleaner' signal plotted for one of the sensors in Figure 2.15. The Bessel filter was selected since it is common in weighing applications. However, other filters are common as well and may be used.

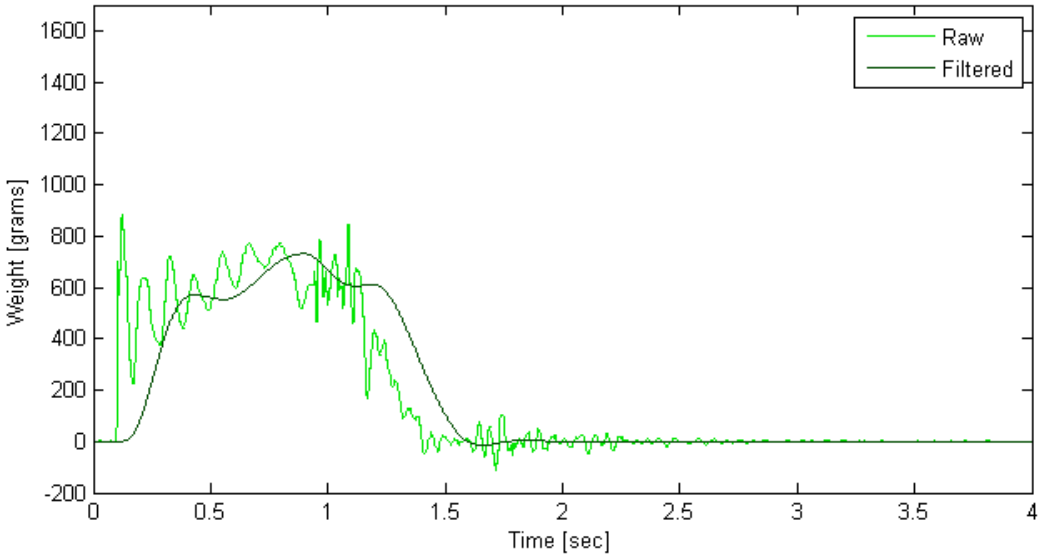

Figure 2.15: Raw vs filtered measurements for a 1 kg box.

1 *kg* Box

Some of the experimental results are presented in Figure 2.16 for illustration. In this set of experiments, it was observed that the sum of the individual peaks of rollers 2 and 3 reached before roller 1 reaches zero is a good estimate of weight. That is because at the instant where the box leaves roller 1, it is fully supported by rollers 2 and 3. The two Figures below show two measurements taken for a 1 kg box. Note that the filters add some delay to the signals and thus the timing difference between rollers is affected.

In mathematical terms, let t_0 = time at which roller 1 equals to zero. Then, the mass estimate m is:

$$m = \max_{t\in[0,t_0]} r_2(t) + \max_{t\in[0,t_0]} r_3(t)$$

where t is time in *seconds*, and $r_2(t)$ and $r_3(t)$ are the mass in *grams* measured by rollers 2 and 3 respectively.

For a weight of 1 kg, the measured weight is 553+480=1033 *grams* and 517+486=1003 *grams*.

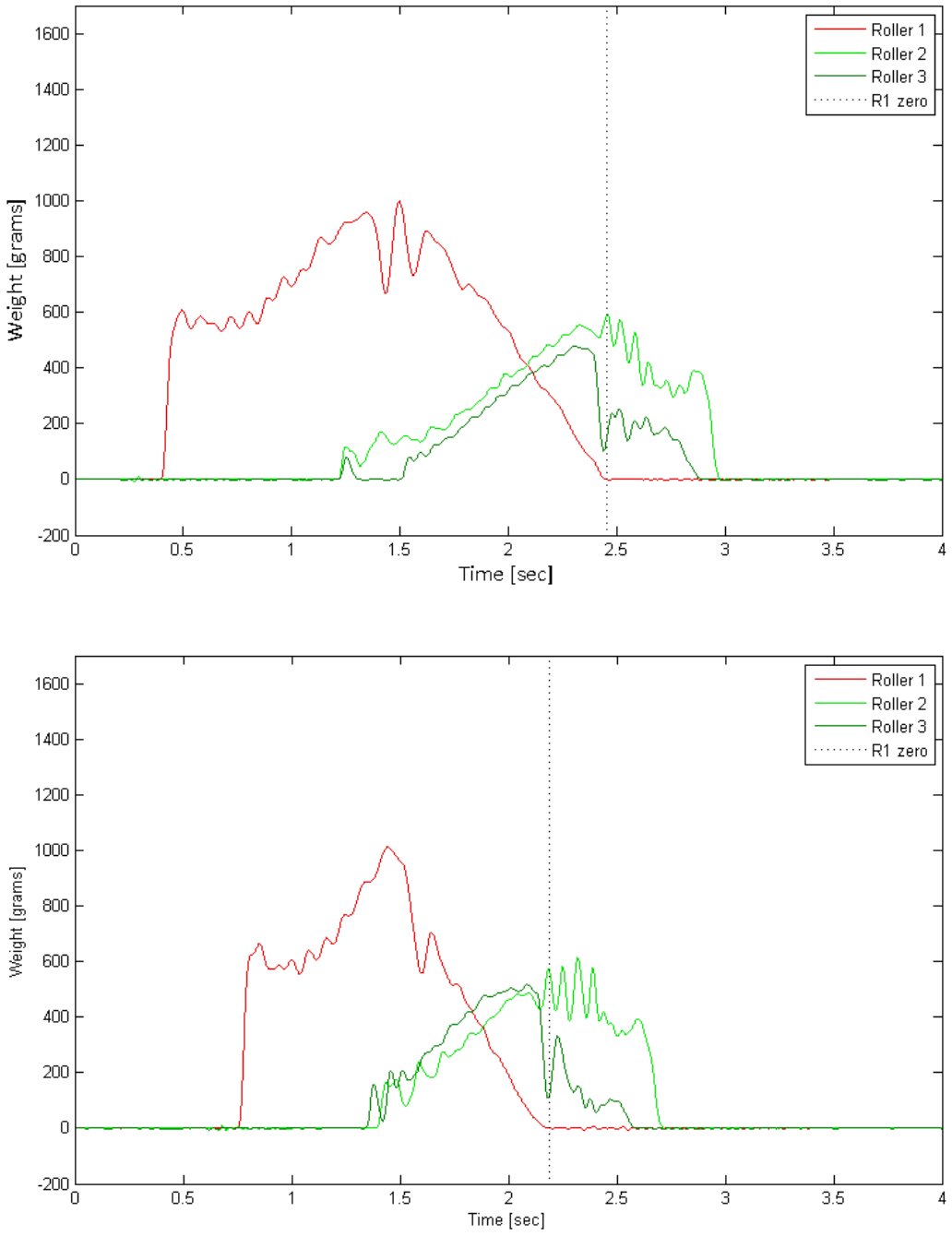

Figure 2.16: Measurements for a 1 kg box.

50 sets of measurement data have been collected and analysed for this case. The cut-off frequency for the filter was adjusted to reduce error. For this set of experiments, a cut-off frequency of 5.5 Hz was used and the box moves at an average speed of roughly 0.2 m/s. Figure 2.17 shows the measurement error distribution. The average error in absolute value is 1.5371% of the actual weight.

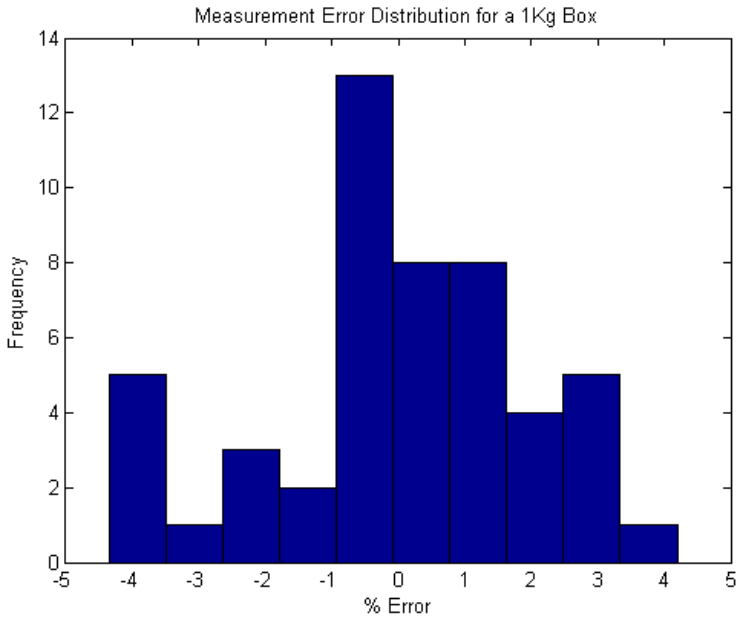

Figure 2.17: Measurement Error for a 1 kg box.

1.59 *kg* Box

The experiment was repeated for 1.59 kg. The measured weights are 884+715=1599 $grams$ and 945+676=1621 $grams$ for the two examples in the Figure 2.18.

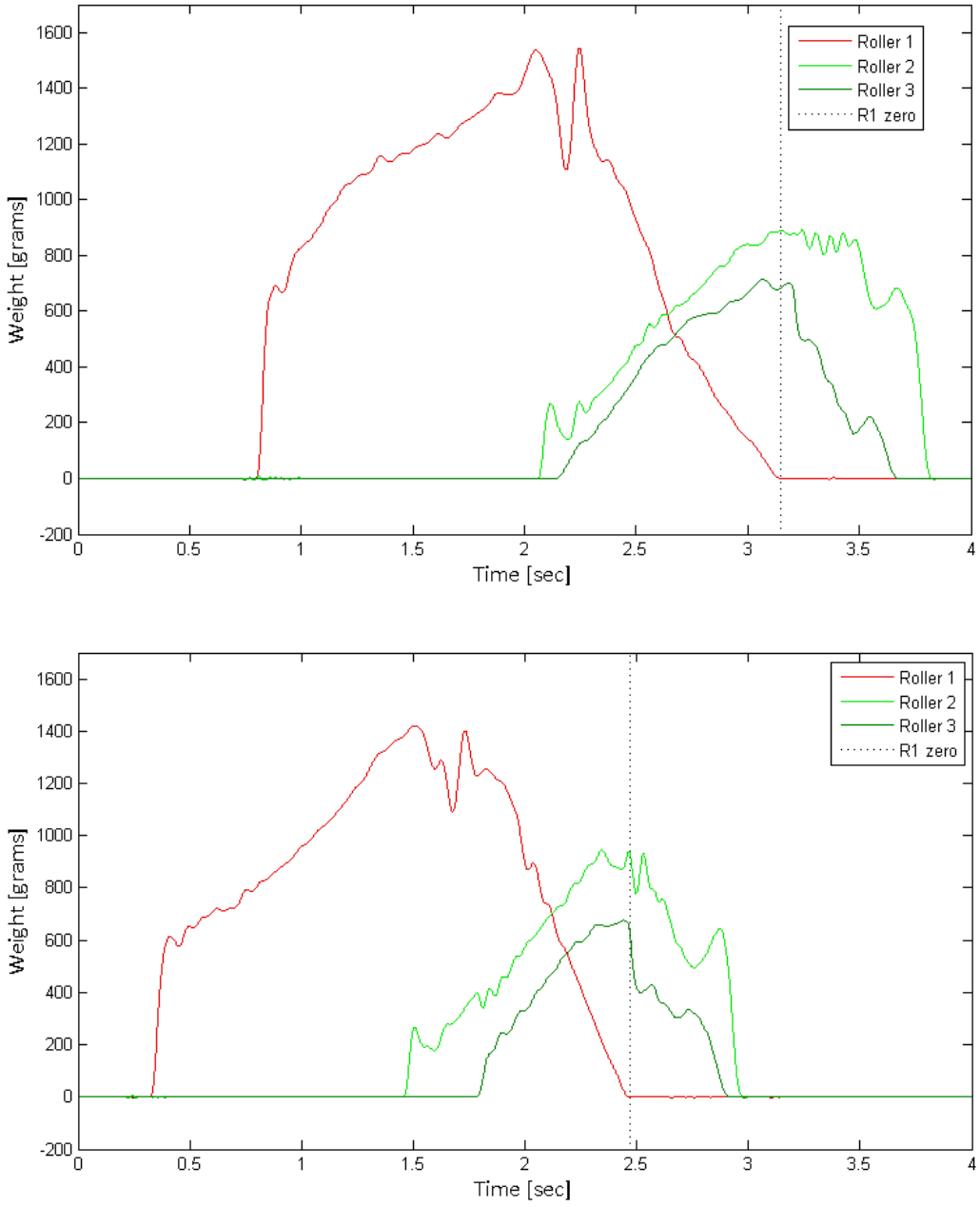

Figure 2.18: Measurements for a 1.59 kg box.

As before, a set of 50 tests is analyzed for the new weight. For this set of experiments, a cut-off frequency of 7.5 Hz was used and the box moves at an average speed of roughly 0.22 m/s. The measurement error distribution is in Figure 2.19. The average error is 1.3527% of the actual weight.

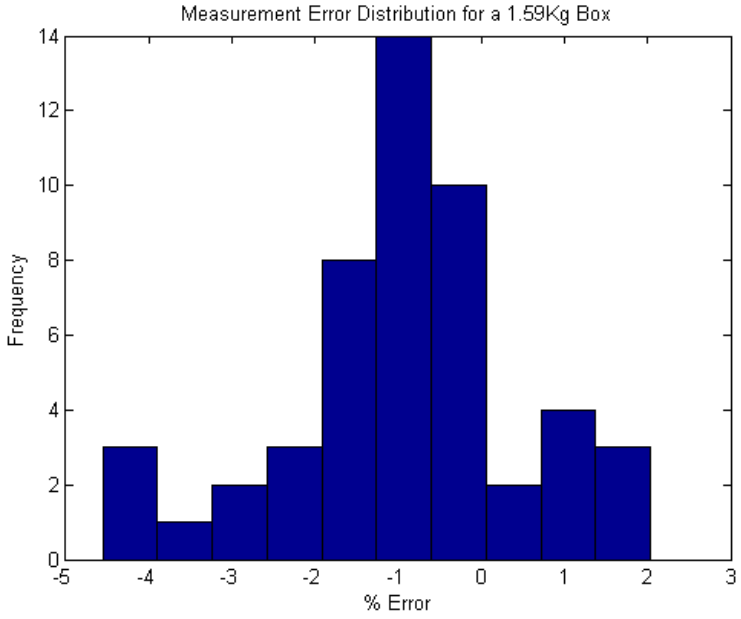

Figure 2.19: Measurement Error for a 1.59 kg box.

4.095 *kg* Box

Similarly, for a weight of 4.095 kg, the measured weights are 2381+1887=4268 $grams$ and 2345+1775=4120 $grams$ in Figure 2.20.

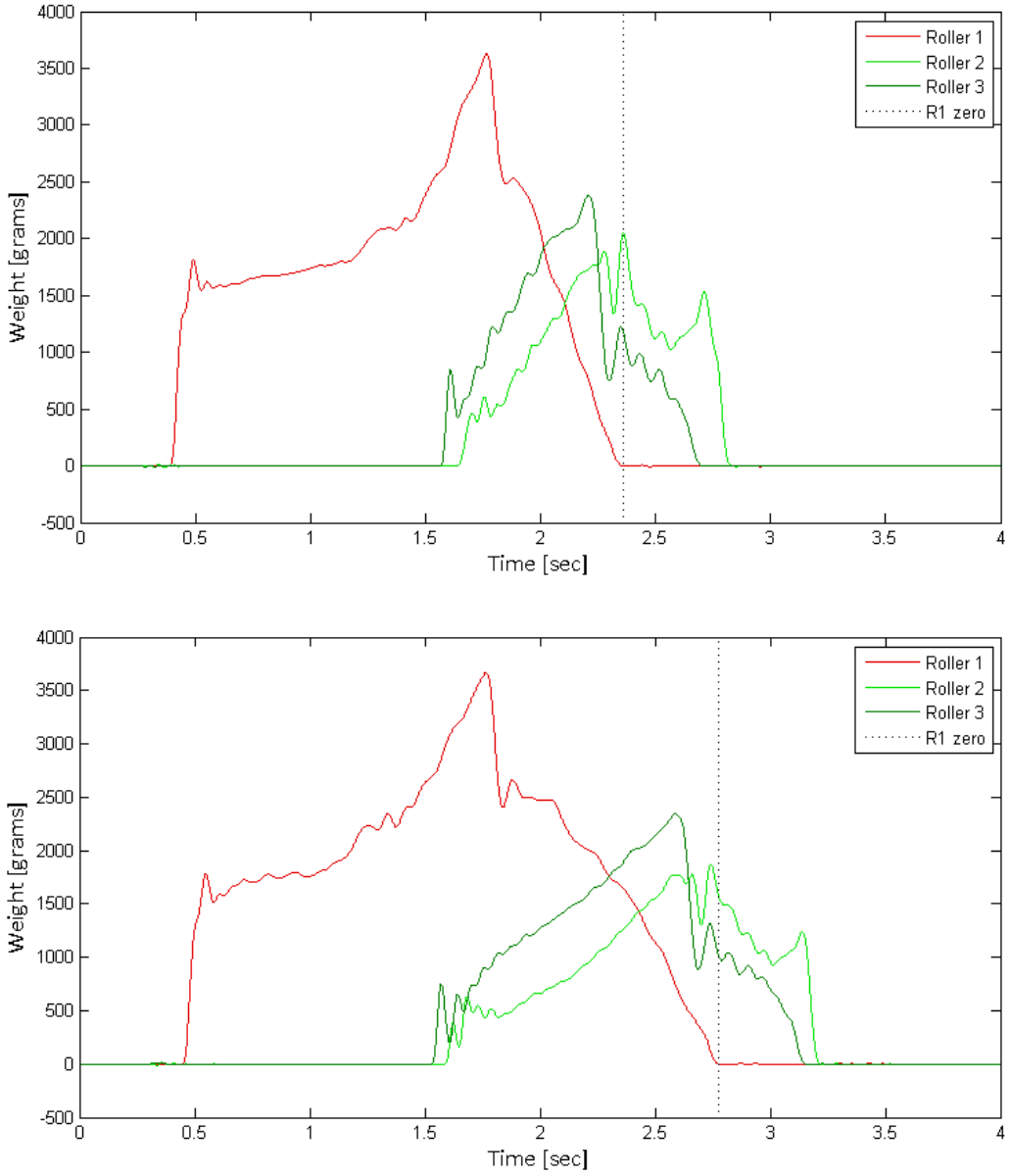

Figure 2.20: Measurements for a 4.095 kg box.

For this set of experiments, a cut-off frequency of 6.5 Hz was used and the box moves at an average speed of roughly 0.29 m/s. Figure 2.21 displays the measurement error

distribution. The average error is 1.3176% of the actual weight.

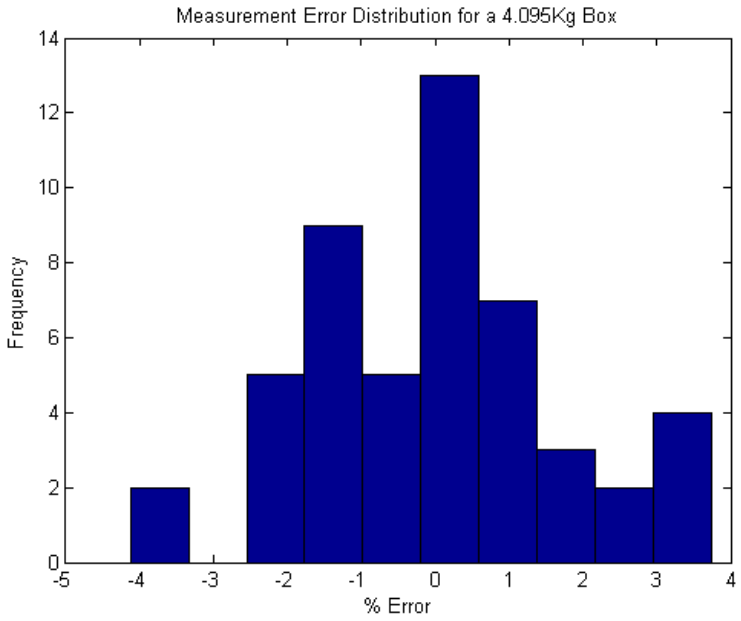

Figure 2.21: Measurement Error for a 4.095 kg box.

1 *kg* Box - Higher Speed

The results for the three different weights have an average error around 1.3-1.5%. However, when the speed of the box increases, the signal becomes noisier resulting in less accurate measurements, see Figure 2.22 for example. Note that this example, in fact, accurately measures the 1 kg weight, but this was not consistent when the experiment is repeated.

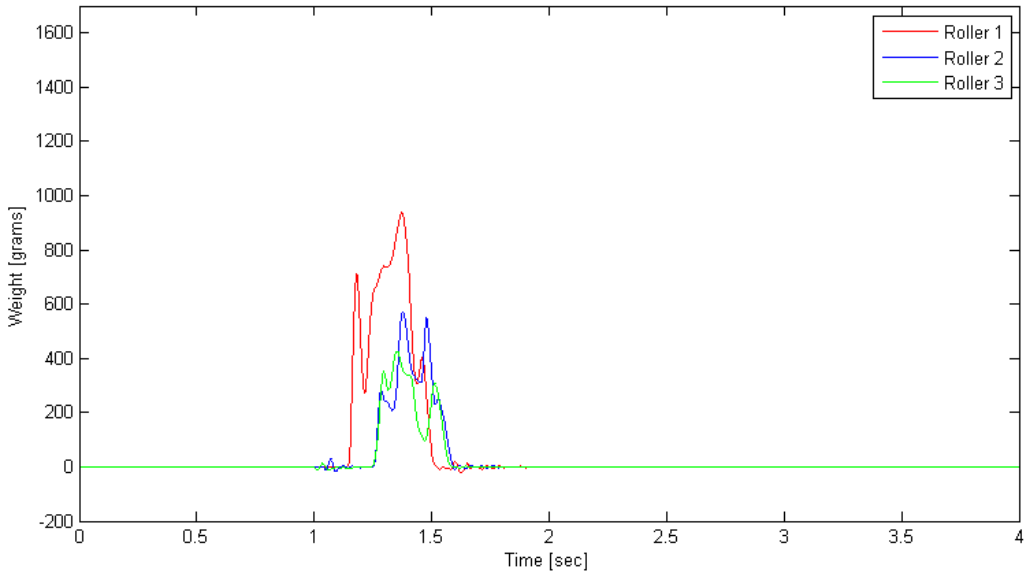

Figure 2.22: Measurements for a 1 kg box moving faster.

The test is repeated 50 times and analyzed with a cut-off frequency of 7.6 Hz for the filter. The box moves at an average speed of roughly 0.5 m/s. The measurement distribution is in Figure 2.23. The average error is 8.2684% of the actual weight.

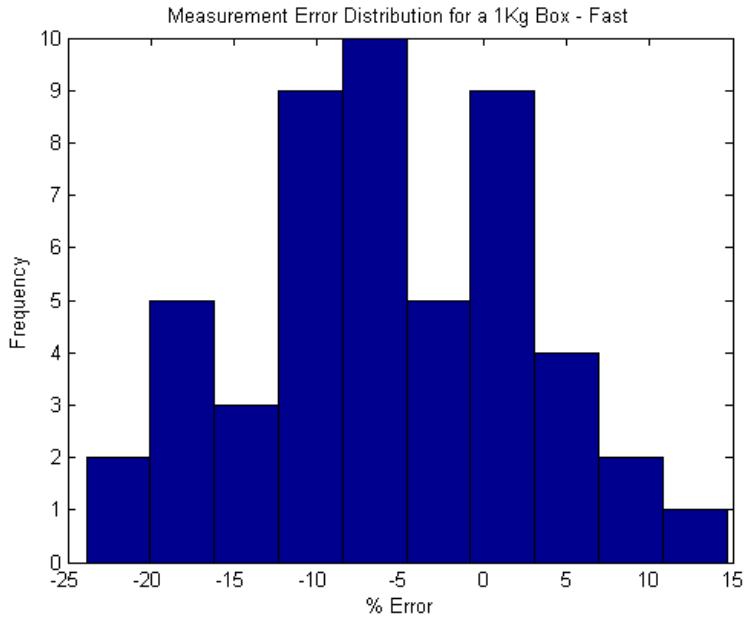

Figure 2.23: Measurement Error for a 1 kg box moving faster.

1 *kg* Box - Incline

Another set is collected for the 1 kg box sliding on an incline (of 23.5 $degrees$). The cut-off frequency is 12 Hz for the filter and the box moves at an average speed of roughly 0.48 m/s. The average error is 11.5318% of the actual weight and the distribution is shown in Figure 2.24.

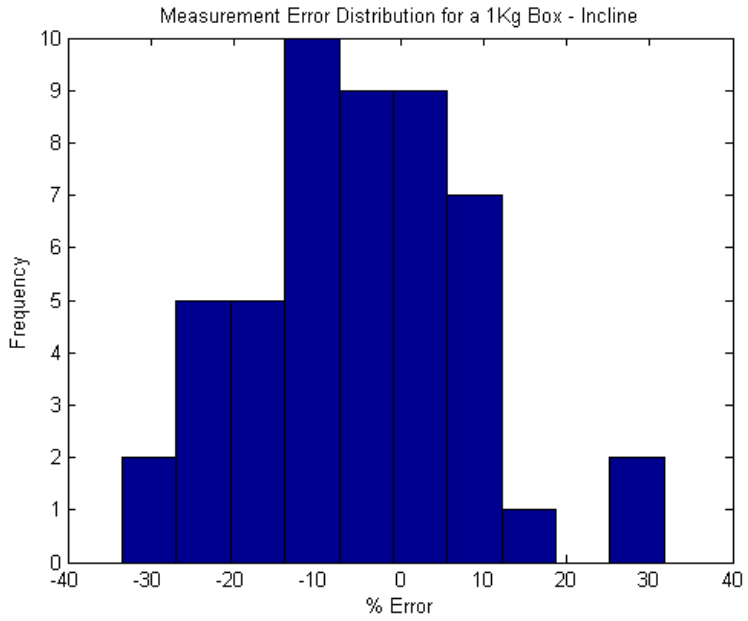

Figure 2.24: Measurement Error for a 1 kg box freely sliding down an incline.

The results are summarized in table 2.1. It can be observed that a cut-off frequency ranging between 5.5 and 7.5 Hz is appropriate to achieve an error less than 1.6% for different weights moving at less than 0.3 m/s. Also, the error increases as the speed of the moving package increases. The different weights used do not seem to affect the average error in the experiments. The error distributions are somewhat asymmetric and can only be roughly fitted into known distributions.

Table 2.1: Summary of small scale proof-of-concept experiments.

Test	**Absolute Average Error (%)**	**Cut-Off Frequency(Hz)**	**Speed (rough, in m/s)**
1 *kg*	1.5371	5.5	0.2
1.59 *kg*	1.3527	7.5	0.22
4.095 *kg*	1.3176	6.5	0.29
1 *kg* Fast	8.2684	7.6	0.5
1 *kg* Incline	11.5318	12	0.48

2.2.3 Results and Discussion

Increasing the supported speed of the boxes on the conveyor will require further improvement. The filters can be tuned and adjusted to increase accuracy based on statistical analysis.

Mechanical Damping

Mechanical damping is recommended to reduce vibrations by the load cells. The vibrations were clearly visible in the experiments and the results. Fluid damped load cells are available in industry for speed weighing and the AG cell has a compatible fluid damping kit that can be used. The speed cell kit, Figure 2.25, costs around $925.

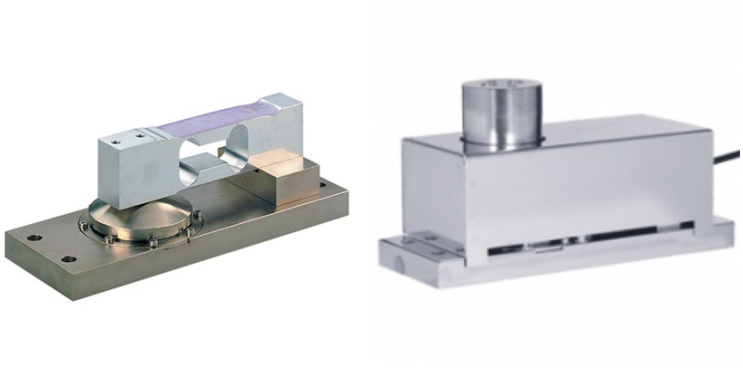

Figure 2.25: SpeedCell fluid damping kit for AG load cells.

Speed Control

Actuation of the wheels/rollers is desired for practical purposes and to control the speed of the conveyor in a manner that achieves accurate weighing in the fastest time. It would be possible to manage the conveyor such that packages move relatively slowly over the load cells without affecting the overall speed of the belt. For example, if the overall speed of the conveyor is 1 m/s, there would be a section that runs at 2 m/s followed by a weight measuring section that runs 0.5 m/s.

Calibration

Further calibration and fine tuning is necessary to reach the desired accuracy in the operating environment. The conditions in the sorting facility and for a line ready prototype will be different than those in the lab. Thus, it is important to calibrate and test when setting up.

Materials and Build

The prototype can be improved mechanically by choosing different build materials, assembly techniques and parts. This will yield better results in terms of noise, vibration and consistency. Also, the load cells should be mounted to align the rollers better horizontally.

2.3 Prototype Design

In order to ensure that objects of different sizes and shapes are conveyed smoothly, belt type conveyors are selected instead of rollers. The size of the conveyor was determined based on package dimension statistical data collected by Purolator. The prototype was designed to be placed connecting two 4 $foot$ wide belts in the shipping company's sorting facility. As a result, the size of the smallest common packages moving on those belts that Purolator wished to accommodate was chosen as the desired width and length of the small belt conveyor. The desired dimensions were between 15 to 20 cms for the width and 25 to 31 cms in terms of length. The target capacity for each belt conveyor scale was selected to be 20 kgs, excluding the scale platform's weight, based on the statistics as well. This design objective requires a small sized drive motor with relatively high torque and matching the larger belt speed of 0.2 m/s. Due to budget constraints and limited options for small belt conveyors with the desired torque in the market, we decided to design the conveyors in-house. The first prototype, shown in Figure 2.26, was designed and constructed for testing.

Figure 2.26: Prototype for the first iteration of conveyor belt design.

In addition to the high torque and small size requirements, the conveyor design takes into consideration the spacing constraints that come with the grid layout in Figure 2.2. Thus, the conveyor was designed to be compact with a high power brushless DC motor mounted inside a frame and driving a timing pulley with its shaft. The drive pulley in turn drives another shaft-mounted timing pulley via a timing belt. The driven pulley rotates and a flat belt translates this rotational motion into a linear motion causing objects to move across the conveyor. Side shields prevent moving objects from getting stuck in the gaps. It was learnt from the first design iteration that tensioning the belts, which is necessary for smooth uniform motion, can be difficult. A tensioning mechanism was added to overcome this problem. The mechanism allows varying the belt length by tightening and releasing screws and, as a result, the belt can be tensioned after assembly. The conveyor is mounted on a load cell through an assembly consisting of four mounting brackets, a plate, nuts and bolts. The assembled design is illustrated in Figure 2.27.

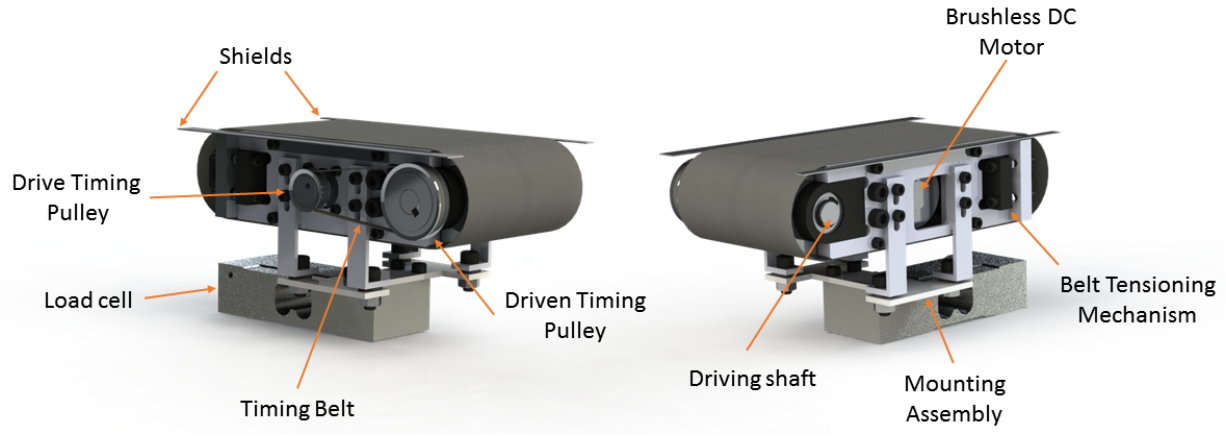

Figure 2.27: Rendered isometric views of the second conveyor belt design iteration mounted on a load cell.

The conveyor dimensions were constrained by those of the driving motor. Brushless DC motors offer a high torque to size performance ratio, and so, 57HBL01A brushless dc motors by Smart Automation were purchased for the design. The motors have a rated torque of 0.14 $N.m$ and rated speed of 4000 rpm for a good price. A gearbox with a 1/13 reduction ratio is selected for the motors. The resulting conveyor system is capable of transporting 20.5 kgs at a speed of 0.8 m/s, meeting the design objectives. The final design is 308.18 mms long, 191 mms wide and 126.8 mms high from the load cell as shown in Figure 2.28.

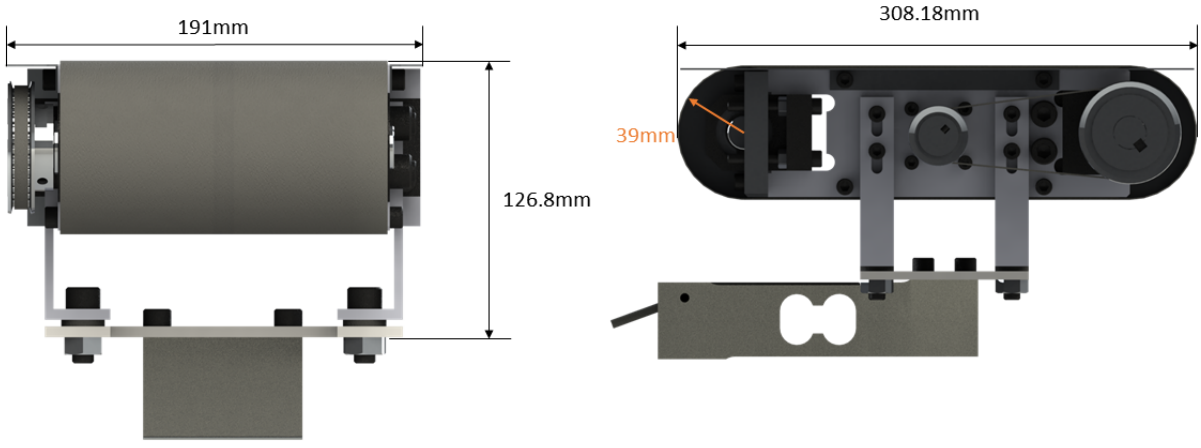

Figure 2.28: Dimensions of the conveyor belt assembly.

The overall weighing machine is depicted in Figure 2.29. A t-slot aluminium frame with custom aluminium mounting bars supports the load cell/conveyor assemblies. A vision system is mounted on the top of the frame to track and dimension packages. The t-slot design allows easier assembly, alignment, grid gap adjustment, and frame design changes if needed. Mounting feet with dampening pads were mounted on each leg of the frame to reduce noise from the floor and to align the load cells horizontally with the ground. 75 *kg* AP series load cells from Scaime were found suitable for the prototype. The sensors offer a C3 accuracy class sufficient for the application, meet the requirement for platform dimensions (load cells have a specification for the maximum allowable weighing platform size), have a rugged construction, are off-center load compensated and have a good value for the price. ENod4-C signal conditioning circuits are purchased to amplify, condition and digitize the low voltage analog load cell signals. The interfacing is done as described in subsection 2.2.1 but with the eNod4-C instead of the eNod3-C.

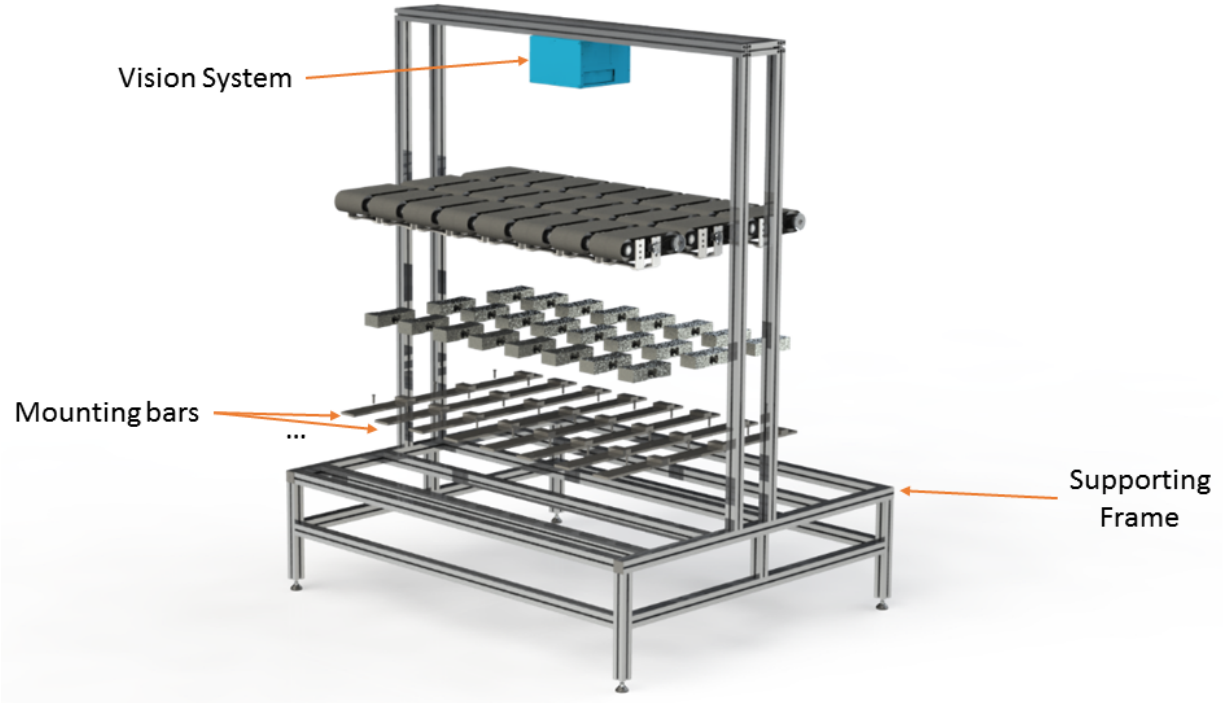

Figure 2.29: Rendered exploded view of the complete weighing machine solution.

Due to the high number and power of motors in the system, it is necessary to design a cost-effective safe power supply system. Figure 2.30 is a schematic of the proposed circuit design. The Figure includes recommended wire gauges and some of the specifications for

the parts. Each of the motors is controlled and powered by a WS-2406 motor driver from Smart Automation. The driver allows varying the motor speed with a potentiometer or a digital input. One Meanwell LRS-350-36 DC power supply can safely power two of the motor drivers. A fused AC power plug can power three of the power supplies when connected to an AC outlet.

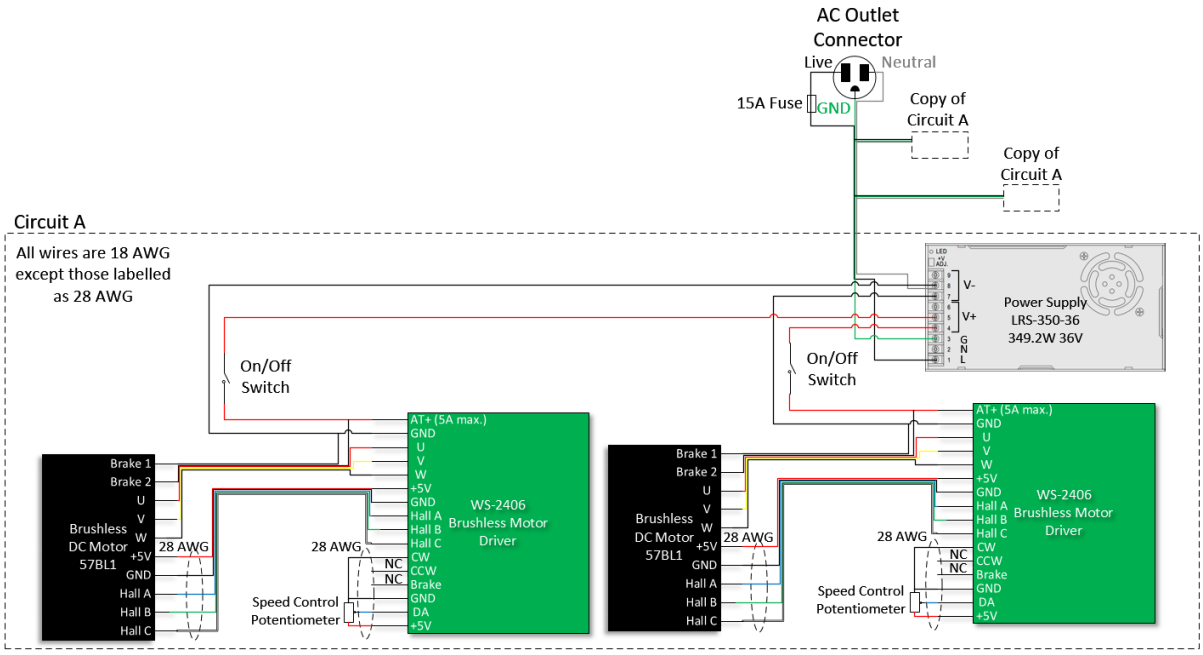

Figure 2.30: Wiring schematic of the brushless DC motors.

One of the requirements to achieve CSA (Canadian Standards Association) safety approval is to properly enclose the power supplies and drivers. Thus, an enclosure is selected and the box is designed to fit 3 power supplies and 6 drivers. The box, Figure 2.31, has a panel at the front with slots for speed controlling potentiometers and ON/OFF motor switches for manual control. The back of the box will be closed with motor and power cables emerging through drilled holes that have fitted cable grips as needed.

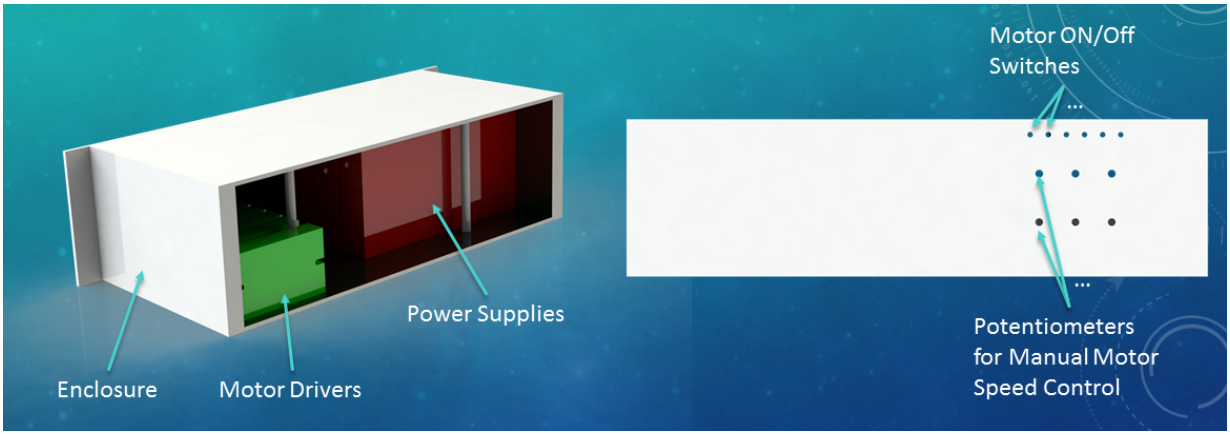

Figure 2.31: Rendered images of the electrical box when the back is open and its front panel.

In order to associate the sensor measurements with the corresponding packages, a sensor that continuously tracks the position of the measurands is required. Usually in checkweigher applications, a simple light sensor detects the entry of the measurand onto the weighing belt and another detects its exit. However, this is not practical in the proposed machine. To effectively detect the positions of individual packages crowding the weighing grid, a light curtain, or other sensor, has to be placed at the entrance and exit of each element of the grid. This comes with the disadvantage of having a large number of sensors blocking the passage of moving items (since items may be large enough to span several elements of the grid at a time). Instead, the vision system in Figure 2.32 from Tricolops Technologies Inc. is utilized. The system is capable of dimensioning any object statically and at speeds below 0.5 m/s. The performance of the system was evaluated experimentally in Chapter 4.

Figure 2.32: Object detecting and dimensioning vision system.

Chapter 3

Filtering Approach

There are many different approaches to filtering in weighing applications. For the novel weighing machine, a discrete time-variant low-pass filter is designed similar to that in [16] for fast and accurate measurements. The filter was selected instead of a model-based approach due to numerous potential sources of noise in an industrial environment that may deteriorate the performance of a model-based approach. To illustrate that this is true and in order to test the effectiveness of the filter for the machine, the filter is implemented in MATLAB and compared to the results of a model based filter and a simple averaging filter. The model of the belt conveyor scales in the machine has been derived. Filtering algorithms paired with zero adjustments and calibration are implemented to estimate the weights of the packages based on the output.

3.1 The Discrete Time-variant Low-pass Filter

From [16], a discrete time-variant low-pass filter can be designed by cascading first-order IIR (Infinite Impulse Response) filters of the form:

$$y_i(n) + a_k(n)y_i(n-1) = b_k(n)[y_{i-1}(n) + y_{i-1}(n-1)] \tag{3.1}$$

where:

$i \in \{1, \ldots, k\}$ with k being the number of filters in cascade;

$n \in \{1, \ldots, N\}$ with N denoting the time the weighed object starts leaving a weighing conveyor;

The input signal of the first filter in the cascade $y_0(n)$ is the output of the load cell;

The output signal of the cascade $y_k(n)$ is the weight estimate at time n (it will contain a delay compared to raw data). The estimate at the last sample N can be taken as the estimated mass of the weighed object;

The coefficients $a_k(n)$ and $b_k(n)$ are chosen using

$$a_k(n) = \frac{f_c(n) - \frac{c_k}{\pi\Delta}}{f_c(n) + \frac{c_k}{\pi\Delta}}, b_k(n) = \frac{1 + a_k(n)}{2}, c_k = \sqrt{\sqrt[k]{2} - 1} \tag{3.2}$$

with Δ and $f_c(n)$ as below;

Δ is the sampling period (in *sec*);

$f_c(n)$ is the cut-off frequency chosen such that it gradually decreases towards the end of the analysis/filtering interval. This results in a shorter transient response without affecting disturbance attenuation as explained in subsection 1.3.3. A suitable selection is:

$$f_c(n) = f_\infty + (f_0 - f_\infty)\lambda^{\frac{n-1}{\alpha(N-1)}}, \alpha > 0, \lambda > 0 \tag{3.3}$$

The selection yields a k-th order low-pass filter with an exponentially decaying cut-off frequency. The frequency decreases from an initial value of f_0 towards a limiting value of f_∞ at a rate determined by α. The effect of α is illustrated in Figure 3.1. λ can be arbitrarily chosen to be a small number such as 0.01.

f_∞ and k define the time-invariant behaviour of the filter after f_c converges. Thus, their values can be chosen based on the frequency analysis of the load cell readings. For example, in Figure 3.2, the fast Fourier transform (FFT) is applied to sample experimental load cell measurements and the results are plotted. Based on that plot, the two parameters are selected to amplify the useful low frequency amplitudes and attenuate the remaining noisy high frequency components. The frequency-amplitude plot of the resulting fixed filter is included in the figure to show that it matches the experimental plot.

The other two parameters f_0 and α are related to the time-variant aspect of the filter. One approach to achieve optimal filter settings is to associate a performance metric with each choice of f_0 and α. The performance metrics are selected to achieve certain design goals for the weighing machine such as weighing speed, weighing accuracy, repeatability and others. This cost is then minimized for some training data sets and at a certain belt speed j to find the appropriate parameter values. Here, we will select two components of the metric:

$$\xi_j^* = \arg\min_{\xi} \{\delta_j(\xi) + \eta_j(\xi)\}, \xi = [f_0, \lambda]^T \in \mathbb{R}^2 \tag{3.4}$$

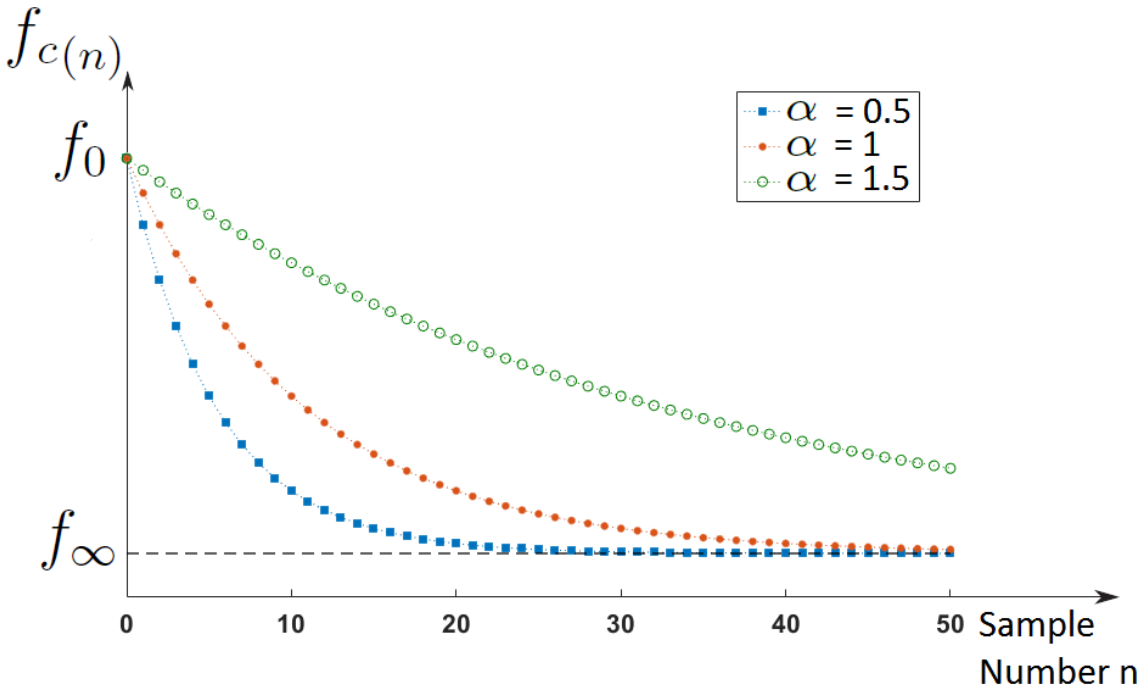

Figure 3.1: Plots of the cut-off frequency $f_c(n)$ for $\lambda = 0.01$, $N = 50$, and 3 different values of α.

The first quantifies measurement accuracy in term of mean error $\mu_{ij}(\xi)$ normalized by a maximum permissible value μ_{imax}, where i corresponds to a test load m_i:

$$\delta_j(\xi) = \max\left\{\frac{\mu_{ij}(\xi)}{\mu_{imax}}, i = 1, 2, ...\right\} \tag{3.5}$$

For the proposed machine, we set the goal of not exceeding $\pm 0.02\%$ mean error of the rated capacity of the load cells $C_n = 75\ kg$. This corresponds to a permissible error of ± 15 *grams*. The second component of the performance measure reduces the transient response:

$$\eta_j(\xi) = \max\left\{\frac{\eta_{ij}(\xi)}{N}, i = 1, 2, ...\right\} \tag{3.6}$$

$\eta_{ij}(\xi) \in [1, N]$ is the settling time of the step-like response of the filter. It is determined by finding the shortest time after which the filter output settles within the desired $\pm 15 grams$ of error. If the absolute value of the mean error is higher than $15 grams$, $\eta_j(\xi)$ will become

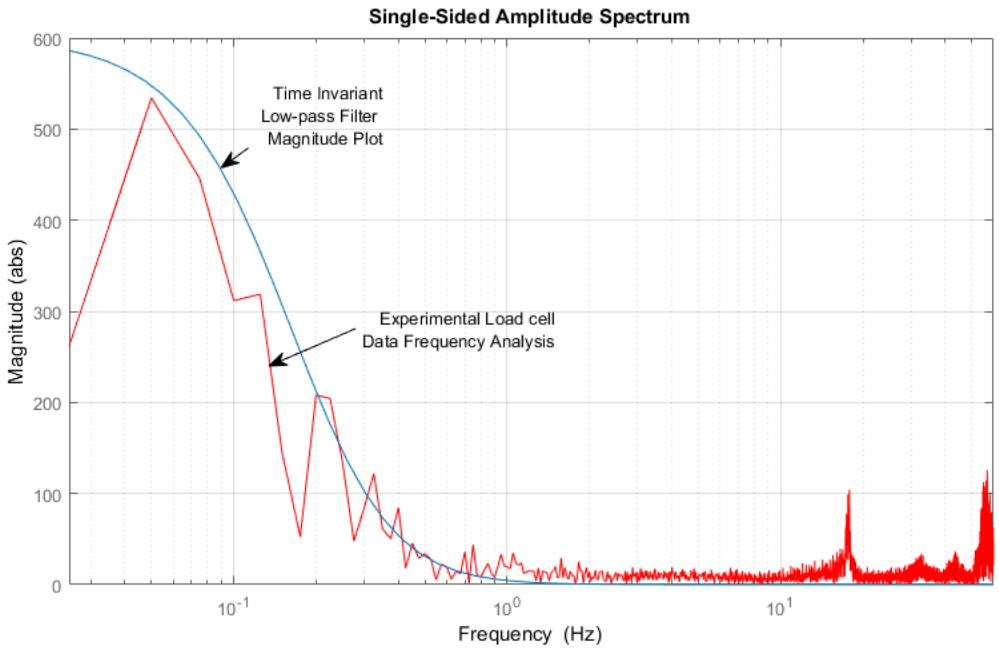

Figure 3.2: Selection of the filter parameters f_∞ and k based on the frequency domain analysis of the load cell data.

equal to 1, heavily penalizing the filter that does not meet accuracy requirements. An example showing the filtered response of the described filter vs the unfiltered response for a weighing cycle $[1, N]$ is shown in Figure 3.3. N may be replaced with a tunable variable to minimize spacing between packages as we will discuss in section 4.1. For the novel weighing machine, optimisation will be done for the first component, accuracy, only due to simplify our preliminary design goals.

3.2 Model-based Estimation

As discussed in section 1.3.1, the most common load cell model in the literature is that of a simple mass-spring-damper (MSD) we showed in Figure 1.14. One reason for the effectiveness of the model is that single point load cells have a dual cantilever beam design which is sensitive to shear and resistant to bending. As a result, the majority of the displacement caused by the weight will be in the direction of the vertical motion θ which

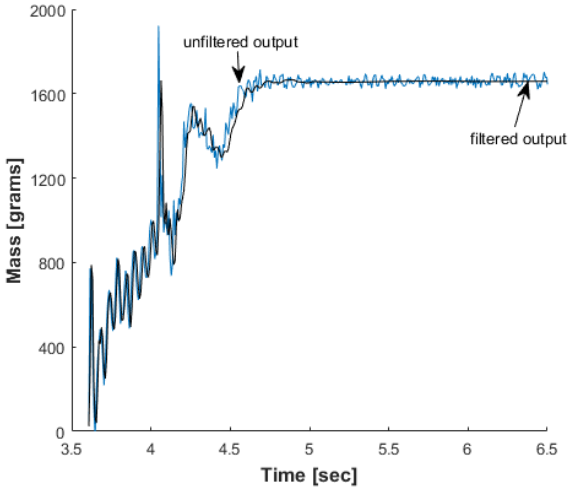

Figure 3.3: Example of unfiltered and filtered responses for an experimental weighing cycle.

matches the one dimensional aspect of the model. Load cells are also designed to behave like springs rendering the second order oscillator model suitable. From Newton's second law ($\sum \vec{F} = m\vec{a}$), the following time-variant differential equation describing the MSD model can be written:

$$w(t)g = (w(t) + m_l)\ddot{\theta}(t) + c\dot{\theta}(t) + k\theta(t) \tag{3.7}$$

where:

$w(t)$ is the mass of the measurands carried by the load cell scale in kgs, which varies with time;

g is the gravitational acceleration constant approximated as 9.81 m/s^2;

m_l is the empty load cell equivalent mass in kgs, constituted of the mass of the scale platform (belt conveyor in this case) and the contribution of the load cell beam. A common estimation for m_l is $m_l \approx 0.23 mass_{loadcell} + mass_{scale}$ [25];

$\theta(t)$ is the vertical relative equivalent displacement in meters of the mass m_l with respect to the static position when $w(t) = 0$. $\theta(t)$, the strain in the load cell's strain gauge, the sensed Wheatstone bridge voltage, and the measurand mass are all proportional to each other in the steady state;

$\dot{\theta}(t)$ and $\ddot{\theta}(t)$ are the first and second derivatives of $\theta(t)$ in m/s and m/s^2 respectively;

c is the equivalent linear damping coefficient, in kg/s, of the load cell in the measuring direction;

k is the equivalent linear stiffness, in N/m, of the load cell in the measuring direction.

Equation 3.7 can be rewritten in state space form as:

$$\dot{x}(t) = \begin{bmatrix} \dot{\theta}(t) \\ \ddot{\theta}(t) \end{bmatrix} = \begin{bmatrix} 0 & 1 \\ -\frac{k}{w(t)+m_l} & -\frac{c}{w(t)+m_l} \end{bmatrix} x(t) + \begin{bmatrix} 0 \\ \frac{g}{w(t)+m_l} \end{bmatrix} w(t) \tag{3.8}$$

Then, equation 3.8 has the form:

$$\begin{cases} \dot{x}(t) = A(t)x(t) + B(t)w(t) + z(t) \\ y(t) = Hx(t) + v(t) \end{cases} \tag{3.9}$$

where $z(t)$ and $v(t)$ are added to model the stochastic mechanical disturbances and the electrical measurement noise respectively;

$y(t)$ is the estimated mass of the measurand in kgs, and $H = \begin{bmatrix} k_c & 0 \end{bmatrix}$ with $k_c = k/g$, in kg/m as the coefficient giving the mass estimate from the displacement $\theta(t)$.

This model was used while developing the filtering algorithms to generate simulated load cell data. The simulation involves packages moving on a grid of load cells mimicking the function of the proposed machine. The generated data was helpful in verifying the algorithms. However, due to similarities with experimental results, we omitted the simulation results and only present the experimental ones. Figure 3.4 shows an example comparing simulated and experimental load cell output. The output was produced for a typical checkweigher such as the one shown in Figure 1.12 experimentally and in simulation for an equivalent system. The simulated response is very close to the experimental one with one clear difference. The noisy ramp behaviour preceding the step behaviour is distorted in the experimental case. This is because of variations in the instantaneous velocity of the moving measurand.

From the model in equation 3.7, an identification-based approach to mass estimation is derived for comparison. Since the steady state is of importance in this approach, the transient response of the weighing cycle in Figure 3.3 is ignored. The resulting cycle corresponds to the time n_0 when the weight starts being fully supported by the scale till N. Thus, $w(t)$ in eq. 3.7 becomes a time invariant unknown mass M to be estimated. Detecting the transients in a response similar to the unfiltered one in Figure 3.3 can be done by finding the settling time. The value of the last sample is taken as the steady state value and the settling time is defined as the time where the load cell output settles to within 2% of this value. Then, the mass-spring-damper model in its differential equation form becomes:

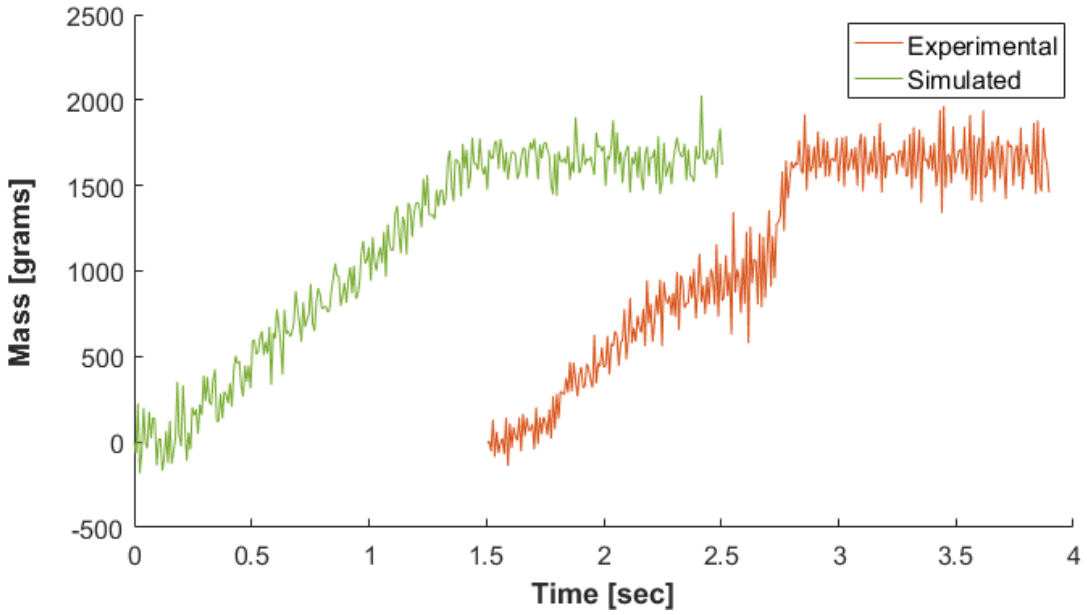

Figure 3.4: Comparing simulated and experimental load cell outputs for a checkweigher system.

$$(M + m_l)\ddot{\theta}(t) + c\dot{\theta}(t) + k\theta(t) = Mgu(t) \tag{3.10}$$

where $u(t)$ is the input function, in this case, it can be taken as a step function.

Following the steps in [47], the Laplace transformation of the above equation assuming non-zero conditions is

$$\Theta(s) = \frac{Mg}{k}U(s)\frac{{\omega_n}^2}{s^2 + 2\zeta\omega_n s + {\omega_n}^2} + \frac{\theta(0+)s + \dot{\theta}(0+) + 2\zeta\omega_n x(0+)}{s^2 + 2\zeta\omega_n s + {\omega_n}^2} \tag{3.11}$$

where

$$U(s) = L\left\{u(t)\right\} = \frac{1}{s}, \quad \zeta = \frac{c}{2\sqrt{k(M + m_l)}}, \quad \omega_n = \sqrt{\frac{k}{M + m_l}}$$

The voltage output of the load cell(s) are processed via an ADC before reading. Thus, the output is discrete while the input is a piecewise continuous and constant (staircase) input. An exact discretization for such an input is a zero-order hold continuous-discrete conversion method. Applying the method yields the following $\mathcal{Z}$-transform:

$$\Theta(z) = \frac{Mg}{k}U(z)\frac{b_1^* z^{-1} + b_2^* z^{-2}}{1 + a_1 z^{-1} + a_2 z^{-2}} + \theta(0+)\frac{1 + \alpha z^{-1}}{1 + a_1 z^{-1} + a_2 z^{-2}} \tag{3.12}$$

with $U(z) = \mathcal{Z}\left\{u(k)\right\} = 1/(1 - z^{-1})$; a_1, a_2, b_1^*, and b_2^* are parameters that depend on the sampling time T, ζ and ω_n; and α is an expression of $\theta(0+)$, $\dot{\theta}(0+)$, a_1 and a_2.

Since $U(z)$ is known and the displacement $\theta(n)$ is directly proportional to the load cell readings $x(n)$ by the constant k_c, equation 3.12 can be rewritten in a more compact form:

$$X(z) = k_c U(z)\frac{\theta(0+) + b_1 z^{-1} + b_2 z^{-2}}{1 + a_1 z^{-1} + a_2 z^{-2}} \tag{3.13}$$

where

$$b_1 = \frac{Mg}{k}b_1^* + (\alpha - 1)\theta(0+) \quad \text{and} \quad b_2 = \frac{Mg}{k}b_2^* - \alpha\theta(0+)$$

Applying the final value theorem on eq. 3.13:

$$\lim_{i\to\infty} x(iT) = \lim_{z\to 1}(z-1)X(z) = k_c\frac{\theta(0+) + b_1 + b_2}{1 + a_1 + a_2} \tag{3.14}$$

Similarly, applying the same theorem to $k_c\Theta(s)$ in eq. 3.11 will give a steady state value of $k_c Mg/k = M$. Thus, since this value is equal to that in eq. 3.14, the mass M can be estimated using

$$M = \frac{b}{1 + a_1 + a_2} \tag{3.15}$$

where $b = \frac{k}{g}(\theta(0+) + b_1 + b_2)$.

According to [47], the system parameter estimates $\widehat{b}(N), \widehat{a}_1(N)$, and $\widehat{a}_2(N)$ can be obtained using the least squares (LS) method assuming the noisy measurement is filtered with a low-pass filter at the output. Note that b is being estimated instead of $\theta(0+)$, b_1, and b_2 individually since $u(n)$ is a step function. In other words, since $u(n)$ has a constant value of 1 for all samples, eq. 3.13 can be written as the difference equation:

$$x(n) = -a_1 x(n-1) - a_2 x(n-1) + b$$
$$\text{for} \quad n \geq 2.$$

The parameters are placed in a vector $\widehat{\boldsymbol{\theta}}(N) = [\widehat{b}(N), \widehat{a}_1(N), \widehat{a}_2(N)]^T$. The LS method gives:

$$\widehat{\boldsymbol{\theta}}(N) = [\boldsymbol{\Phi}^T\boldsymbol{\Phi}]^{-1}\boldsymbol{\Phi}^T\boldsymbol{x} \tag{3.16}$$

where $\boldsymbol{\Phi} = [\boldsymbol{\phi}(n_0), \ldots, \boldsymbol{\phi}(N)]^T$ is a matrix consisting of the regression vectors $\boldsymbol{\phi}(n) = [1, -x(n-1), -x(n-2)]^T$, $n = n_0, \ldots, N$, and $\boldsymbol{x} = [x(n_0), \ldots, x(N)]^T$.

Finally, the mass can be estimated with:

$$\widehat{m}(N) = \frac{\widehat{b}(N)}{1 + \widehat{a}_1(N) + \widehat{a}_2(N)} \tag{3.17}$$

As a third approach to use for comparison, we simply take the average of the data samples starting after the steady state is achieved and until the weighing cycle ends at time N.

Chapter 4

Experimental Verification

In this chapter, the proposed novel weighing machine is evaluated for the three different filtering approaches described in chapter 3; namely the discrete time-variant low-pass filter, the parameter estimation method, and the simple averaging of the steady state measurements. Limitations in terms of allowable spacing between packages are discussed. Zero adjustment and calibration done are also described. In order to isolate sources of noise, two main experiments are conducted. In the first one, the idea of having a grid of scales with moving packages is tested without the noise contribution of motors. In the second experiment, the first weighing conveyor belt prototype is evaluated without the influence of the grid concept.

4.1 Minimum Spacing Requirements between Packages

Initially, the problem we wished to address was to dynamically measure the weight of a package moving in a non-singulated and non-spaced environment. However, due to accuracy constraints, it was not possible to formulate a solution with existing sensor technologies without some spacing requirements. The solution proposed in this work is capable of addressing the problem effectively but with some spacing necessary between packages. This inconvenience creates the need for equipment to separate packages available in the market such as hold-and-release mechanisms, robotic arms, and singulators. On the other hand, it still solves the other aspects of the problem, including increased weighing throughput with

a smaller plant floor footprint for the equipment. In this section, the spacing requirements are discussed.

In Figure 4.1, the minimum horizontal and vertical spaces between two packages are defined as S_x and S_y respectively. The width W and length L are indicated for each of the scale platforms. Also, the horizontal and vertical gaps between adjacent scale platforms are labelled as G_x and G_y respectively. The packages are moving along the horizontal axis in the figure.

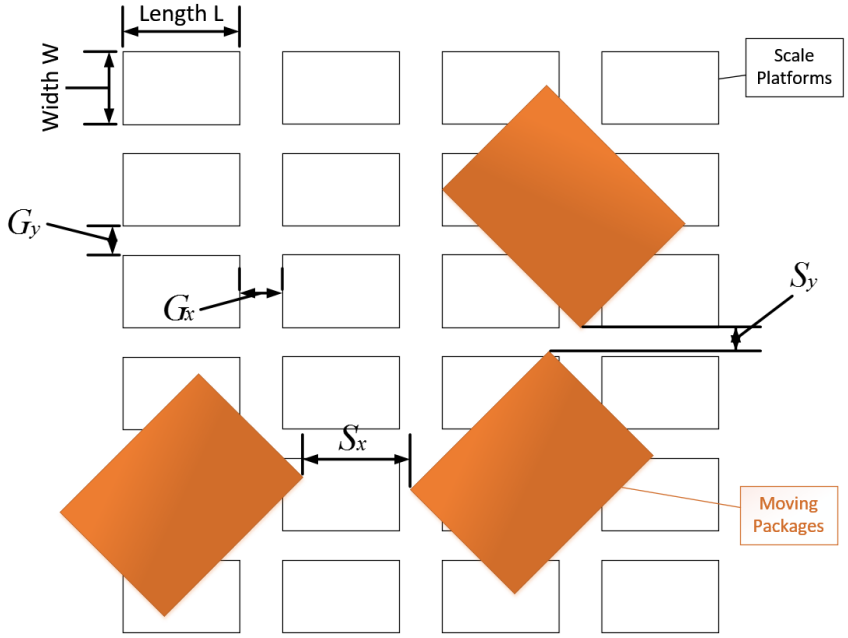

Figure 4.1: Spacing requirements for novel weighing machine.

If S_y between two packages is at least greater than the width W, then it is guaranteed that the two packages will not overlap on the same weighing platform due to S_y. Then, the first requirement is that $S_y \geq W$ to avoid weighing issues. W can be designed to be small to decrease the spacing requirement S_y; however, this increases the cost of the machine since more conveyor scales are needed. Also, smaller belt conveyors can be more difficult to design.

The second requirement is a bit more involved to formulate since motion occurs along the x-axis. Assuming the worst case for S_x which is zero, a package will have a steady

state weighing time T_{ss} in seconds (useful weighing signal) with:

$$T_{ss} = \frac{G_x}{v_{belt}} - T_s \tag{4.1}$$

where G_x is as previously defined in meters, v_{belt} is the constant speed of the belts in m/s and T_s is the settling time of the load cell response in seconds.

By design, all of the variables in equation 4.1 can be controlled with some trade-offs and constraints. G_x can be increased to reduce spacing requirements at the expense of potential issues conveying packages (packages may get stuck in the gaps) and increasing mechanical noise due to impact. The magnitude of this cost will depend on the dimensions of the packages being conveyed; packages with a longer dimension along the x-axis and with more evenly distributed weight will be less affected by bigger gaps. The speed of the belts v_{belt} will depend on the overall design of the line the machine will be part of. A slower speed will yield better accuracies for a minimal S_x but can be a bottleneck in terms of throughput if it is slower than the rest of sections of the line. T_s depends on the choice of load cells and mechanical design. Load cells with a better response time tend to be more expensive. It is also possible to purchase more accurate, but more expensive, load cells, such as C6 accuracy ones commonly used in checkweighers.

4.2 Zero Adjustment and Calibration

Load cells are typically adjusted by an offset to compensate for the weight of the scale it carries as well as mechanical and electrical drift offsets. After the adjustment, the cell should read a reference mass measurement of zero $grams$. On a constantly running weighing system, this adjustment is done frequently. As a result, automatic zero adjustment should be done whenever possible while the system is on-line and the load cell scale is unloaded. To find the offset, a simple low-pass discrete time filter is implemented, due to noisy measurements even when unloaded, by cascading IIR filters of the form:

$$y_i(n) + a_k y_i(n-1) = b_k[y_{i-1}(n) + y_{i-1}(n-1)] \tag{4.2}$$

where all the variables are the same as in equation 3.1, except that a_k and b_k are fixed in this case. They are selected by setting $f_c(n)$ to a constant value f_{adj}. Another difference is that time is defined for the period during which the scale unloaded. f_{adj} can be selected similar to f_∞ based on the frequency analysis of the mass sensor output during the unloaded state.

Load cells are also frequently calibrated off-line. This can be done using the eNodVIEW software and one to three calibration weights. The known mass of the weight(s) is input into

eNodVIEW, the corresponding weight(s) is placed on the load cell when prompted (repeat the last two steps if using another weight), and the software automatically programs the eNod4-C controller to constantly output the calibrated readings and saves this information in memory.

The vision system also needs to be calibration whenever a mechanical adjustment is done to the system. This is done by placing a flat surface spanning the area where packages are dimensioned for reference. Then, the user prompts the vision system's software to calibrate and the process is complete. The software will also show the area in which dimensioning occurs. To increase, or decrease, the dimensioning area, the camera may need to be raised, or lowered, in height.

4.3 Experiment 1: Static Scale Grid with Moving Packages

4.3.1 Setup

The designed weighing machine in Figure 2.29 is fully constructed and assembled with the exception of the conveyor belts. Instead of the conveyor belts in an 8 by 3 grid layout, rectangular pieces of compressed wood are mounted as the scale platforms to form a 3 by 4 grid of detached scales. The pieces have dimensions similar to those of the designed conveyor belts. In the beginning of each experimental repetition, the box sits outside of the grid attached to a strong fishing line. The other end of the fishing line is wrapped around a pulley driven by a brushless DC motor. Data is collected from the unloaded and pre-calibrated scales for zero adjustment. When the motor is turned on, it will pull the package feeding it to the grid causing dynamic weight measurements as the moving package is supported by different elements of the grid. The motor is attached to a stand with adjustable height to ensure that the line is parallel to the ground and does not cause any lift affecting sensor readings. At the end of the experiment, the package sits on the fourth row of scales. Since dynamic weighing is under evaluation here, the readings of the fourth row of scales are not taken into consideration in mass estimation. The camera captures the position and dimensions of the package. The described setup is illustrated in Figures 4.2, 4.3, and 4.4. Expected sources of noise are electrical noise, environmental and mechanical vibrations due to motion and impact as the packages overcome the gaps between the scales.

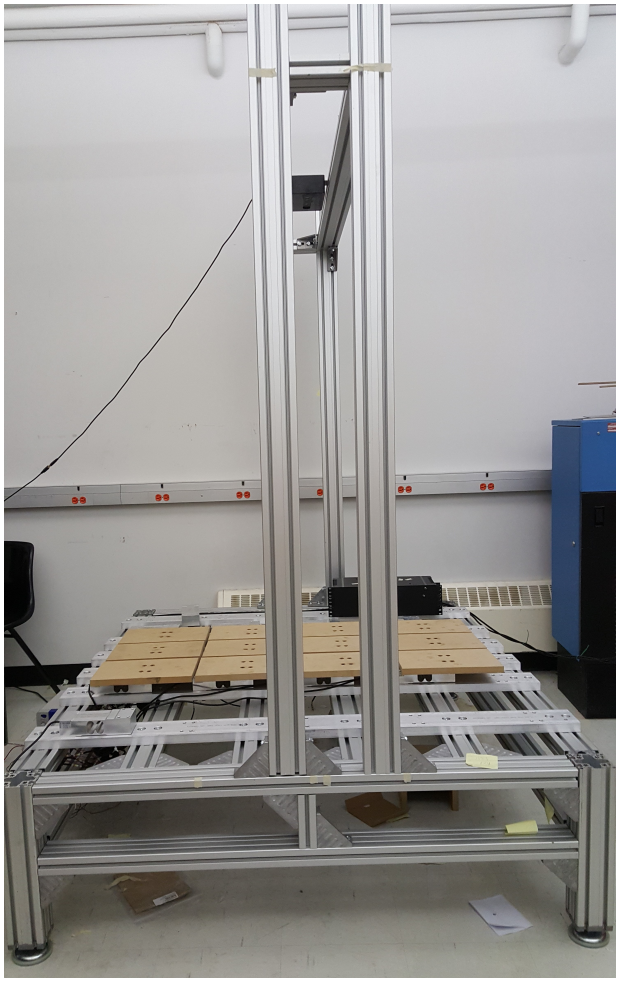

Figure 4.2: Constructed weighing machine.

Figure 4.3: Package is pulled with a string along the weighing grid.

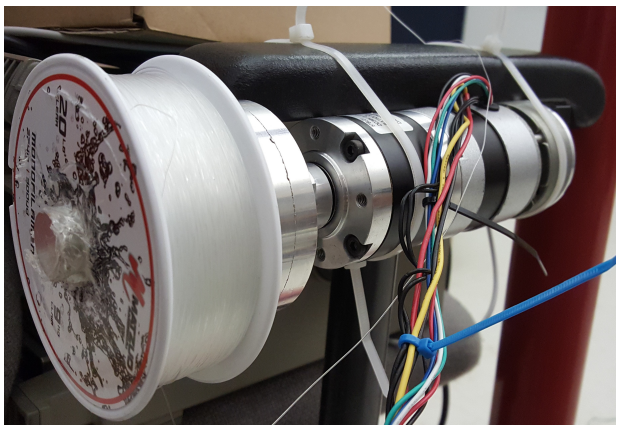

Figure 4.4: Motor with a string pulley moving packages across the grid.

The experiments are repeated for 4 different test weights, and 4 different speeds. For one of the weights, the tests are repeated but with a different package orientation to check if there is any noticeable effect. The weights are measured statically as well for comparison. Two different box sizes are used throughout the experiments to test the camera's dimensioning capability as well. The performed experiments are summarized in Table 4.1.

Table 4.1: Experimental setup 1.

Test Weights	**Box Sizes**	**Different Orientations**	**Speeds**
1,650 *grams*	Small ($\sim$27cm x 15cm x 10cm)	2	4 (between 0.1 and 0.6 m/s)
2,047 *grams*	Big($\sim$32cm x 30cm x 29cm)	1	4 (between 0.1 and 0.6 m/s)
4,620 *grams*	Big($\sim$32cm x 30cm x 29cm)	1	4 (between 0.1 and 0.6 m/s)
10,076 *grams*	Big($\sim$32cm x 30cm x 29cm)	1	3 (between 0.1 and 0.4 m/s)
All above	-	-	Static

4.3.2 Results

Based on camera data collected during the experiments outlined in table 4.1, it was found that the camera dimensioning error does not exceed an average of 2.41 *cms*. In this experiment, the objects were cuboids and thus volume, or volume error, can be calculated by multiplying the three dimensions, or errors of the three dimensions. For other shapes, the camera approximates objects as convex hulls. An example of the camera data is plotted in Figure 4.5. Each coloured rectangular shape represents the package at a different time sample with a circle marking its center. The black rectangles represent the weighing platforms. The increase in velocity does not seem to affect the error. The results are summarized in Figure 4.6.

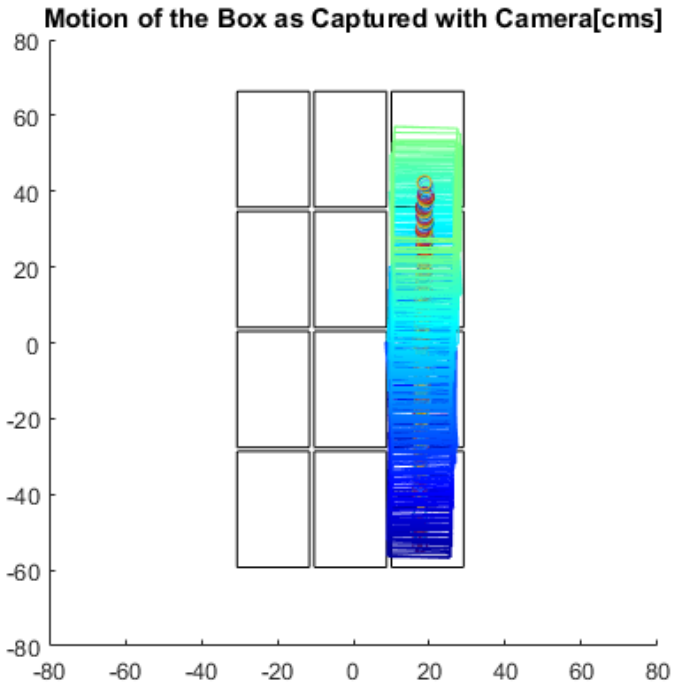

Figure 4.5: Stop motion capture of the 2D approximation of the convex hull of the moving packages.

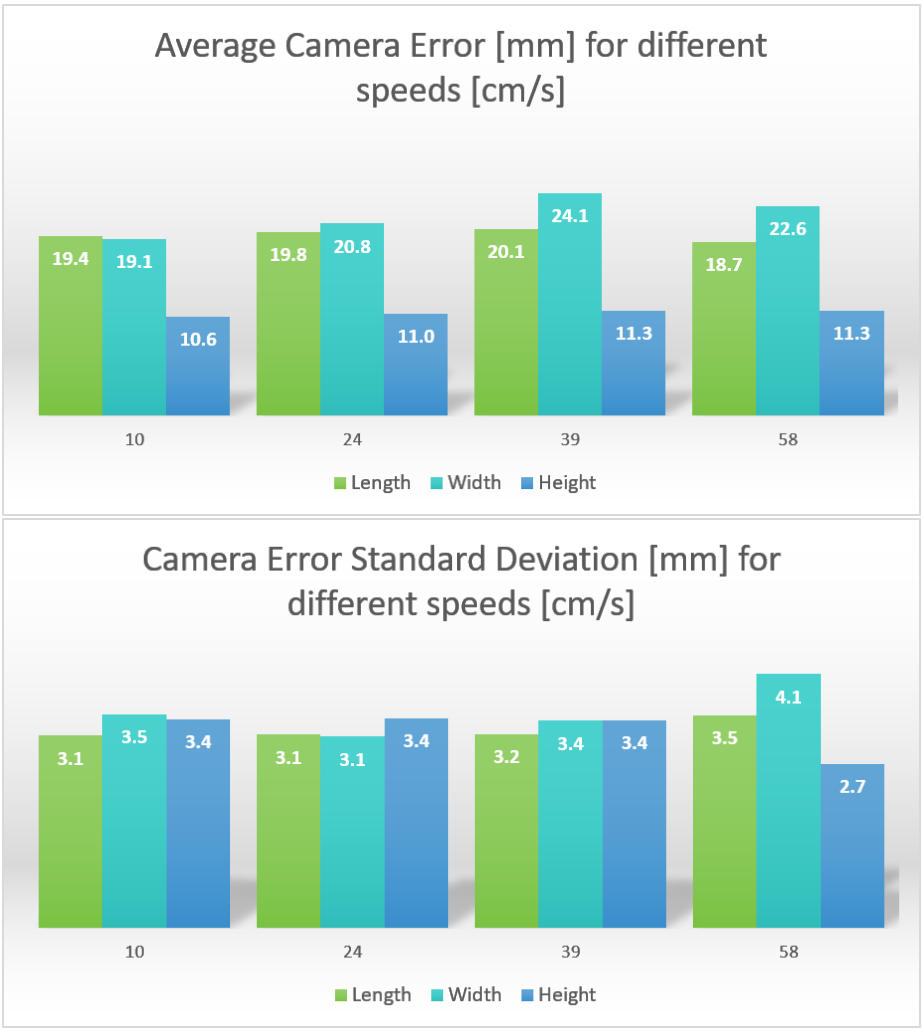

Figure 4.6: Camera average dimensioning error and standard deviation for four different speeds.

Another observation can be made when examining the effect of different package orientation in table 4.2. When the package is oriented such that it is moving along its length in orientation 1, the camera underestimates the length of the package due to the motion. Since the error is positive when the box is static, the underestimation results in a reduction in the length's dimensioning error. Similarly, when the package is moving along its width in orientation 2, the error in dimensioning the width becomes lower and that of the length becomes smaller compared to orientation 1. The height dimensioning error is not

significantly affected by the orientation. Thus, motion causes a reduction in estimation of the dimensions parallel to the direction of velocity.

Table 4.2: Comparing the effect of orientation on camera dimensioning error.

Set	**Speed #**	**Average Dimensioning Error** $[mm]$		
		Length	**Width**	**Height**
Orientation 1	1	7.83	22.39	9.82
	2	9.86	26.00	11.65
	3	12.62	26.23	11.78
	4	13.08	23.43	11.10
Orientation 2	1	27.54	14.87	9.41
	2	25.65	11.27	12.03
	3	26.56	18.51	13.01
	4	23.98	15.81	12.35

For the same set of experiments, the load cell data is collected and processed as described in chapter 3. The optimal filter settings are listed in table 4.3 with $k^* = 3$ and ${f_\infty}^* = 0.2\ Hz$ for all speeds. The average error and standard deviation for the three filtering methods: time-variant low pass filter, averaging and parameter estimation methods are plotted in Figure 4.7. The time-variant low pass filter does not exceed the target error of 15 *grams* in all of the weighings while the other methods fail in some. Note that the average error for static weighings, which represents the best possible performance attainable for dynamic weighings, was 2.825 *grams* with a standard deviation of 2.29 *grams*.

Table 4.3: Optimal filter settings for different speeds in experiment 1.

Speed $[cm/s]$	**10**	**24**	**39**	**58**
$\boldsymbol{f_0}^*[Hz]$	138	140	2	130
$\boldsymbol{\alpha}^*$	2.3	1.8	0.7	1.1

Figure 4.7: Experiment 1: weighing error for the three filtering methods at different speeds.

Next, to determine whether the dimensioning accuracy of the camera is sufficient, the time during which the signal is at a steady state value is compared to the maximum delay caused by errors in dimensioning. The reasoning is that delays can cause cropping of the useful steady state load cell samples when the camera and weight sensor data are synchronized, and as a result, jeopardizing weighing accuracy. It is found, as shown in Figure 4.8, that the there a sufficient amount of steady state data to tolerate the maximum camera delay. Thus, the time-variant low pass filter and the camera yield good performance.

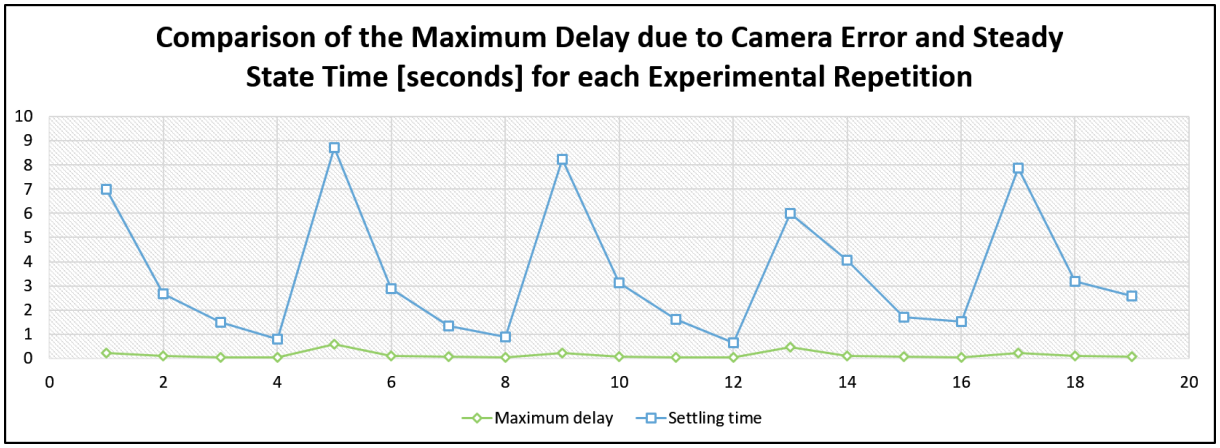

Figure 4.8: The steady state exceeds time delay caused by dimensioning error for all experimental repetitions.

4.4 Experiment 2: Conveyor Belt Scale Evaluation

4.4.1 Setup

In this set of experiments, a single conveyor belt scale prototype is tested. The conveyor belt in Figure 2.26 is mounted on a load cell. A test mass sits on a wooden in-feed platform and a test weight package is manually fed for weighing, see Figure 4.9. The tests are repeated for four different weights (3166, 591, 1867 and 1650 *grams*) at ten different speeds. The same box size is used in all repetitions. The three different filtering methods are implemented and the results are compared. The length of the box is close to the length of the conveyor which will make the weighing more challenging. Electrical noise, environmental and mechanical vibrations due to motion and the running motor are expected to be the main sources of noise.

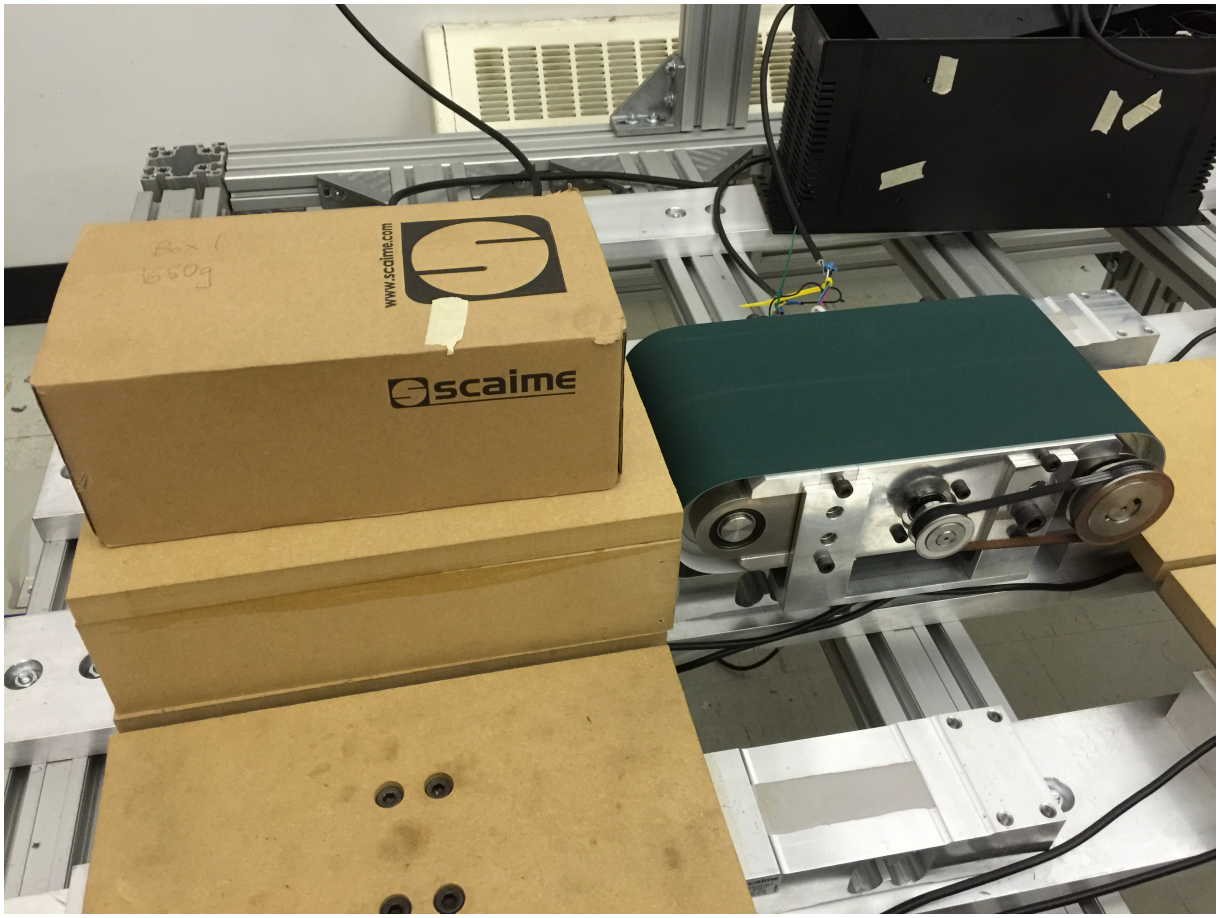

Figure 4.9: The package is pushed onto the moving weighing conveyor for weighing.

4.4.2 Results

As before, the optimal parameters $k^* = 3$ and ${f_\infty}^* = 0.2$ Hz are implemented for all speeds and the remaining two optimal parameters are listed in table 4.4 for each belt speed.

Table 4.4: Optimal filter settings for different speeds in experiment 2.

Speed $[mm/s]$	**46**	**130**	**200**	**273**	**300**	**340**	**450**	**470**	**500**	**600**
$\boldsymbol{f_0}^*[Hz]$	62	126	5	150	75	10	115	120	136	124
$\boldsymbol{\alpha}^*$	0.7	0.9	3.8	0.7	0.8	2.5	0.9	1	0.9	1.1

Figure 4.10 summarizes the results. Despite the difficulty in weighing due to the relatively large length of the package, the time-variant filter succeeds in meeting the average error requirement for all speeds and outperforms the other two methods. These methods meet the requirement at speeds below 0.4 m/s but begin to fail at higher speeds.

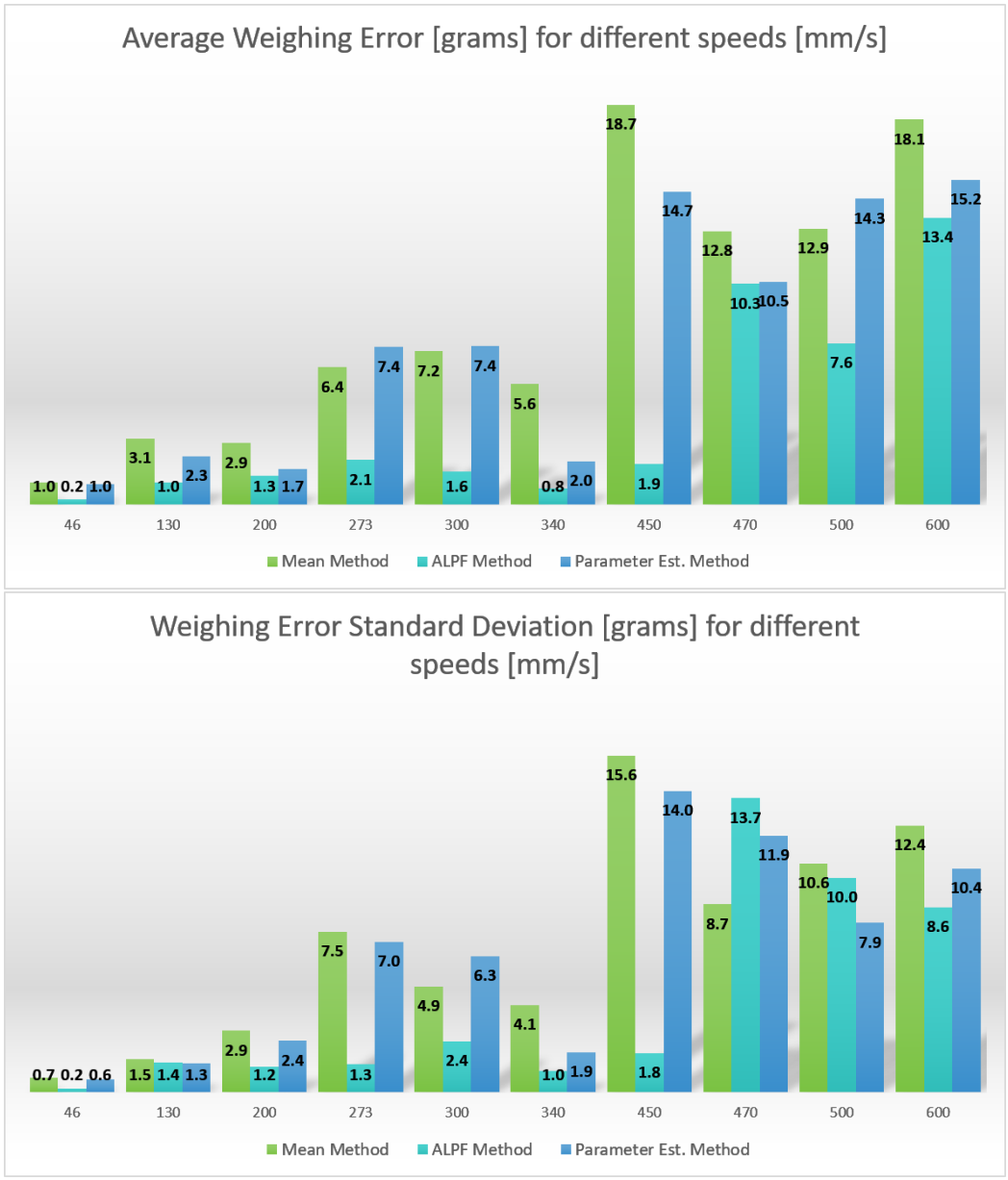

Figure 4.10: Experiment 2: weighing error for the three filtering methods at different speeds.

4.4.3 Discussion

The weighing error increased in general as the speed increased for all methods. This is a common result in related research literature and can be attributed to the higher levels of noise associated with higher speeds. When the system runs faster, the driving motor produces more noise and the moving parts create more mechanical vibrations affecting the load cell signal. Another source of noise that increases with velocity is impact occurring as packages are transferred from one scale to the other. Also, there are less steady-state data samples which are helpful in finding a better mass estimate.

As expected, the averaging method has the worst performance since it is easily influenced by biased noise. The parameter estimation method has the second worse performance compared to the time-variant low-pass filter for the same reason. In fact, a parameter estimation is cascaded with a low-pass filter in literature such as in [47]. The paper states that in most cases, if a low-pass filter is not cascaded into the system, satisfactory results are not guaranteed. However, adding a low-pass filter introduces limitations as discussed in section 1.2. Another factor to the success of the time-variant low-pass filter is that its parameters are optimized based on experimental performance. This comes at the price of requiring more extensive tuning and calibration. On the other hand, results that are more accurate and robust to unpredictable industrial environment noise can be worth the effort.

Chapter 5

Conclusion and Future work

As a general comment on the dynamic weighing research research literature, it would valuable to have a resource that systemically compares the different filtering approaches for dynamic mass measurement. The comparison will facilitate choosing the best filter since each paper compares their new method to a limited number of other ones.

Our novel weighing machine consisting of a grid of decoupled platforms and a vision system has a good potential in effectively weighing non-singulated objects while in motion. Detailed design description of the machine including early stage prototypes and a second full scale prototype were presented. Some separation equipment is needed to create some spacing necessary for correct weighing. An alternate approach would be to create a novel manipulation technique using the vision system and the grid formation of conveyors to avoid overlap during weighing.

The accuracies and speeds achieved were reasonable for the early stage prototype considering the mechanical design. The full scale prototype was constructed to conduct two experiments testing performance when weighing moving objects on a static grid of scales and with one conveyor belt scale. The designed time-variant discrete time low-pass filter outperformed a parameter estimation model-based approach and a simple averaging approach for both experiments. It also met the mean error requirement of not exceeding an absolute value of 15 $grams$ (corresponding to $0.02\,\%$ of 75 kg, the maximum capacity of the selected load cells). While the results are good for early testing, further development and verification should be done for the fully integrated machine with a grid of conveyor belts. Also, a target average error is not enough to yield a legal-for-trade weighing product. The machine has to be discussed with metrological regulating organizations, such as OIML, to determine adequate performance goals. Commonly, OIML gives recommendations related

to average error, average standard deviation (related to repeatability), test weights, test weight length and others.

Other filtering methods may be implemented in an attempt to improve performance. In addition, the machine has to be tested for different measurand orientations to verify that good performance can be attained regardless of the orientation.

Minimum requirements on spacing between packages exist. However, they can be reduced by making some design trade-offs involving cost, accuracy, target package sizes, design complexity and conveyability.

Later, the system should be tested on an actual line in Purolator's sorting facility for evaluation. This will require extensive testing, calibration, tuning and troubleshooting.

References

[1] Carolyn D Dillian and Carolyn L White. *Trade and exchange: archaeological studies from history and prehistory*. Springer Science & Business Media, 2009.

[2] Peter Zecchin. Industrial weighing systems-a balanced review. *MEASUREMENT & CONTROL*, 36(1):12–12, 2003.

[3] Proto3000 Inc. Handyprobe next™portable optical cmm. Available http://proto3000.com/assets/uploads/Images/ProductImages/Scanners/Pespective_Left_C-Track.png, 2016. [Online; Accessed 9-July-2016].

[4] Shaun Weston. Mettler-toledo shows off new product inspection technology at emballage. Available http://www.foodbev.com/news/mettler-toledo-shows-off-new-product-inspection-technology-at-emballage, November 2014. [Online; Accessed 9-July-2016].

[5] Purolator Inc. Company profile. http://www.purolator.com/en/resources-and-support/about-us/corporate-information/corporate-profile.page? [Online; Accessed 9-July-2016].

[6] Lorie King Rogers. Sortation: Reliability meets scalability. *Modern Materials Handling*, pages 36–39, May 2012.

[7] Karen L. Miller. These holiday shipping tips will deliver good results. Available http://www.buffalonews.com/business/money-smart/these-holiday-shipping-tips-will-deliver-good-results-20131129, December 2013. [Online; Accessed 9-July-2016].

[8] Peter Zecchin. A guide to dynamic weighing for industry. *Measurement and Control*, 38(6):173–174, 2005.

[9] Weighing & Force Measurement Panel. A guide to dynamic weighing for industry. Technical report, The Institute of Measurement and Control, 87 Gower Street, London, England, October 2010. Publication reference number WFMP1010.

[10] LIAD Weighing and Control Systems Ltd. Automating masterbatch production. Available http://www.liad.co.il/news/cost-masterbatch. [Online; Accessed 9-July-2016].

[11] All-Fill International Ltd. All-fill powder filling machines & technology. Available http://www.allfill.co.uk/powder-filling-machines/. [Online; Accessed 3-September-2016].

[12] TIA Technology Pvt. Ltd. Batch weigher. Available http://tiatechnology.in/wp/?page_id=545. [Online; Accessed 3-September-2016].

[13] Ametech Systems Pvt Ltd. Belt weigher. Available http://amstelweighing.com/Belt_Weigher.html. [Online; Accessed 3-September-2016].

[14] Schenck Process Holding GmbH. Belt weigher - multibelt. Available http://www.schenckprocess.com/products/Multibelt-Belt-weighers. [Online; Accessed 3-September-2016].

[15] Intercomp. Container terminal weigh-in-motion scales. Available http://www.intercompcompany.com/newsdesk.php?news_id=25, July 2015. [Online; Accessed 10-September-2016].

[16] Przemysław Pietrzak, Michał Meller, and Maciej Niedźwiecki. Dynamic mass measurement in checkweighers using a discrete time-variant low-pass filter. *Mechanical Systems and Signal Processing*, 48(1):67–76, 2014.

[17] Rudolph Emil Kalman. A new approach to linear filtering and prediction problems. *Journal of Basic Engineering*, 82(1):35–45, 1960.

[18] Toshiro ONO, Koichi KAMEOKA, and Kumeo NAKAJIMA. Studies on dynamic measurement method of mass and weight (part 1): Dynamic weighing method-a. *Bulletin of JSME*, 22(166):497–503, 1979.

[19] M Tariq, W Balachandran, and S Song. Checkweigher modeling using dynamical subsystems. In *Industry Applications Conference, 1995. Thirtieth IAS Annual Meeting, IAS'95., Conference Record of the 1995 IEEE*, volume 2, pages 1715–1722. IEEE, 1995.

[20] M Halimic and W Balachandran. Kalman filter for dynamic weighing system. In *Industrial Electronics, 1995. ISIE'95., Proceedings of the IEEE International Symposium on*, volume 2, pages 786–791. IEEE, 1995.

[21] M Halimic, W Balachandran, M Hodzic, and F Cecelja. Performance improvement of dynamic weighing systems using linear quadratic gaussian controller. In *Instrumentation and Measurement Technology Conference, 2003. IMTC'03. Proceedings of the 20th IEEE*, volume 2, pages 1537–1540. IEEE, 2003.

[22] Mark McGuinness, David Jenkins, and Galkadowite Senaratne. Modelling the physics of high-speed weighing. *Report on the Proceedings of the 2005 Mathematics-in-industry Study Group*, pages 143–162, 2005.

[23] Mirsad Halimic, Aida Halimic, Salah Zugail, and Zayed Huneiti. Intelligent signal processing for electro-mechanical systems. In *Mechatronics and Its Applications, 2008. ISMA 2008. 5th International Symposium on*, pages 1–5. IEEE, 2008.

[24] Jacek Piskorowski and Tomasz Barcinski. Dynamic compensation of load cell response: A time-varying approach. *Mechanical Systems and Signal Processing*, 22(7):1694–1704, 2008.

[25] Giovanni Boschetti, Roberto Caracciolo, Dario Richiedei, and Alberto Trevisani. Model-based dynamic compensation of load cell response in weighing machines affected by environmental vibrations. *Mechanical Systems and Signal Processing*, 34(1):116–130, 2013.

[26] Yuji Yamakawa and Takanori Yamazaki. Simplified dynamic model for high-speed checkweigher. In *International Journal of Modern Physics: Conference Series*, volume 24, page 1360036. World Scientific, 2013.

[27] Yuji Yamakawa and Takanori Yamazaki. Mathematical model of checkweigher with electromagnetic force balance system. *ACTA IMEKO*, 3(2):9–13, 2014.

[28] Christian Diethold and Falko Hilbrunner. Force measurement of low forces in combination with high dead loads by the use of electromagnetic force compensation. *Measurement Science and Technology*, 23(7):074017, 2012.

[29] Wipotec GmbH. Weighing principle. Available http://www.wipotec.com/en/company/weighing-principle/. [Online; Accessed 5-October-2016].

[30] Rudoif Maier and G Schmidt. Integrated digital control and filtering for an electrodynamically compensated weighing cell. *IEEE Transactions on Instrumentation and Measurement*, 38(5):998–1003, 1989.

[31] Phantom Scales LLC. Weighing technology (loadcell types). http://www.laboratory-balances.com/mfr.php. [Online; Accessed 20-November-2016].

[32] Leonhard M Reindl, Alfred Pohl, Gerd Scholl, and Robert Weigel. Saw-based radio sensor systems. *IEEE Sensors Journal*, 1(1):69–78, 2001.

[33] Username: Jakirschner. Surface acoustic wave sensor interdigitated transducer diagram. Available https://en.wikipedia.org/wiki/File:Surface_Acoustic_Wave_Sensor_Interdigitated_Transducer_Diagram.png, December 2010. [Online; Accessed 4-October-2016].

[34] Mirsad Halimic, W Balachandran, F Cecelja, and M Tariq. Adaptive deconvolution approach for estimating the input of checkweighing systems. In *Instrumentation and Measurement Technology Conference, 2003. IMTC'03. Proceedings of the 20th IEEE*, volume 2, pages 1098–1101. IEEE, 2003.

[35] J-SR Jang. Anfis: adaptive-network-based fuzzy inference system. *IEEE transactions on systems, man, and cybernetics*, 23(3):665–685, 1993.

[36] Toshitaka Umemoto, Yuki Sasamoto, Motoyuki Adachi, and Youitirou Kagawa. Improvement of accuracy for continuous mass measurement in checkweighers with an adaptive notch filter. In *SICE Annual Conference, 2008*, pages 1031–1035. IEEE, 2008.

[37] Przemyslaw Pietrzak. Dynamic mass measurement using a discrete time-variant filter. In *Electrical and Electronics Engineers in Israel (IEEEI), 2010 IEEE 26th Convention of*, pages 000151–000155. IEEE, 2010.

[38] A Pawlowski, F Rodríguez, J Sánchez-Hermosilla, and S Dormido. Fast nonstationary filtering for adaptive weighing system. In *2015 IEEE 20th Conference on Emerging Technologies & Factory Automation (ETFA)*, pages 1–6. IEEE, 2015.

[39] Takanori Yamazaki, Yoshiharu Sakurai, Hideo Ohnishi, Masaaki Kobayashi, and Shigeru Kurosu. Continuous mass measurement in checkweighers and conveyor belt scales. In *SICE-ANNUAL CONFERENCE-*, number 1, pages 470–474. SICE; 1999, 2002.

[40] Ryosuke Tasaki, Takanori Yamazaki, Hideo Ohnishi, Masaaki Kobayashi, and Shigeru Kurosu. Continuous weighing on a multi-stage conveyor belt with fir filter. *Measurement*, 40(7):791–796, 2007.

[41] Maciej Niedźwiecki, Michał Meller, and Przemysław Pietrzak. System identification based approach to dynamic weighing revisited. *Mechanical Systems and Signal Processing*, 2016.

[42] M Tariq and W Balachandran. Modelling the dynamic response characteristics of a robot-checkweigher. In *Intelligent Control and Instrumentation, 1992. SICICI'92. Proceedings., Singapore International Conference on*, volume 1, pages 358–362. IEEE, 1992.

[43] Wei Carrigan, Richard Stein, Manoj Mittal, and Muthu BJ Wijesundara. Conformal grasping using feedback controlled bubble actuator array. In *SPIE Sensing Technology+ Applications*, pages 911607–911607. International Society for Optics and Photonics, 2014.

[44] HBM. Oiml accuracy classes explained: Which load cell for which application? Available https://www.hbm.com/en/2637/oiml-accuracy-classes-explained/. [Online; Accessed 20-November-2016].

[45] Scaime. Aluminum single point load cell. Available http://www.scaime.com/en/7/produit/aluminum-single-point-load-cell.html. [Online; Accessed 25-October-2014].

[46] Scaime. Dynamic weighing controller. Available http://www.scaime.com/en/74/produit/dynamic-weighing-controller.html. [Online; Accessed 26-October-2014].

[47] Wei-Qun Shu. Dynamic weighing under nonzero initial conditions. *IEEE transactions on instrumentation and measurement*, 42(4):806–811, 1993.

[48] Janusz Gajda, Ryszard Sroka, Marek Stencel, Tadeusz Zeglen, Piotr Piwowar, Piotr Burnos, and Zbigniew Marszalek. Design and accuracy assessment of the multi-sensor weigh-in-motion system. In *2015 IEEE International Instrumentation and Measurement Technology Conference (I2MTC) Proceedings*, pages 1036–1041. IEEE, 2015.